CHAPTER 16

THE METHOD OF SPHERICAL HARMONICS (P_N-APPROXIMATION)

16.1 INTRODUCTION

For a gray medium (or on a spectral basis) with known temperature distribution (or for the case of radiative equilibrium), the general problem of radiative transfer entails determining the radiative intensity from an integro-differential equation in five independent variables—three space coordinates and two direction coordinates—a prohibitive task. The method of *spherical harmonics* provides a vehicle to obtain an approximate solution of arbitrarily high order (i.e., accuracy), by transforming the equation of transfer into a set of simultaneous partial differential equations (PDEs). The approach was first proposed by Jeans [1] in his work on radiative transfer in stars. Further description of the method may be found in the books by Kourganoff [2], Davison [3], and Murray [4] (the latter two dealing with the closely related neutron transport theory). The *spherical harmonics method* is identical to the *moment method* described in Chapter 15, except that moments are taken in such a way as to take advantage of the orthogonality of spherical harmonics.

The great advantage of the method of spherical harmonics is the conversion of the governing equation to relatively simple partial differential equations. The drawback of the method is that low-order approximations are usually only accurate in media with near-isotropic radiative intensity, and accuracy improves only slowly for higher-order approximations while mathematical complexity increases extremely rapidly. This has prompted several researchers in the neutron transport community, notably Gelbard [5], to develop an approximate spherical harmonics method, known as the *simplified P_N-approximation*, or *SP_N*. While more readily taken to higher order, this method does not approach the exact solution in the limit.

It is a common misconception that the lowest-order P_1-approximation fails in optically thin media: as seen from Fig. 15-2 or Example 16.2 below, when emission from a hot medium is considered, the P_1-approximation goes to the correct optically thin limit but may fail in the optically thick limit. Rather, the P_1-approximation loses accuracy, e.g., when an optically thin medium acts as a radiation barrier between hot and cold surfaces, in the presence of collimated irradiation,[1] etc.

[1]See Chapter 19.

In this chapter we shall first develop the set of partial differential equations for the general P_N-method for one-dimensional plane-parallel media and their boundary conditions.[2] Next we deal in more detail with the most popular P_1-approximation for arbitrary geometries. Then a brief presentation of the P_3 and higher-order approximation is given. This is followed by a description of the SP_N scheme and, finally, the chapter concludes with a discussion of a number of variations on the P_N-approximation that attempt to overcome its inaccuracy in strongly anisotropic situations, most notably the *modified differential approximation (MDA)*, which separates radiation emanating from walls from the radiation emanating from within the medium. While such methods deliver better accuracy, they are no longer the solution to a simple partial differential equation, but also require the evaluation of some integral correction factors.

16.2 GENERAL FORMULATION OF THE P_N-APPROXIMATION

We may think of the radiative intensity field $I(\mathbf{r}, \hat{\mathbf{s}})$[3] at location $\mathbf{r}$ within the medium as the value of a scalar function on the surface of a sphere of unit radius, surrounding the point $\mathbf{r}$. Any such function may be expressed in terms of a two-dimensional generalized Fourier series as

$$I(\mathbf{r}, \hat{\mathbf{s}}) = \sum_{l=0}^{\infty} \sum_{m=-l}^{l} I_l^m(\mathbf{r}) Y_l^m(\hat{\mathbf{s}}), \tag{16.1}$$

where the $I_l^m(\mathbf{r})$ are position-dependent coefficients and the $Y_l^m(\hat{\mathbf{s}})$ are *spherical harmonics*, given by

$$Y_n^m(\theta, \psi) = \begin{cases} \cos(m\psi) P_n^m(\cos\theta), & \text{for} \quad m \geq 0, \\ \sin(|m|\psi) P_n^m(\cos\theta), & \text{for} \quad m < 0, \end{cases} \tag{16.2}$$

that satisfy Laplace's equation in spherical coordinates. Here θ and ψ are the polar and azimuthal angles describing the direction unit vector $\hat{\mathbf{s}}$, respectively, and the P_l^m are *associated Legendre polynomials*, given by

$$P_n^m(\mu) = (-1)^m \frac{(1-\mu^2)^{|m|/2}}{2^n n!} \frac{d^{n+|m|}}{d\mu^{n+|m|}} (\mu^2 - 1)^n. \tag{16.3}$$

We may substitute equation (16.1) into the general equation of radiative transfer, equation (10.24),

$$\hat{\mathbf{s}} \cdot \nabla_\tau I + I = (1-\omega) I_b + \frac{\omega}{4\pi} \int_{4\pi} I(\hat{\mathbf{s}}') \, \Phi(\hat{\mathbf{s}} \cdot \hat{\mathbf{s}}') \, d\Omega', \tag{16.4}$$

where space coordinates have been nondimensionalized using the extinction coefficient, i.e., $d\tau = \beta \, ds$ (as indicated by the subscript τ in ∇_τ). Equation (16.4) requires the outgoing intensity to be specified everywhere along the surface of the enclosure. Equation (16.4) is multiplied by Y_k^n after also expanding the scattering phase function into a series of Legendre polynomials, equation (12.99), followed by integration over all directions. Exploiting the orthogonality properties of spherical harmonics [6] leads to infinitely many coupled partial differential equations in the unknown position-dependent functions $I_l^m(\mathbf{r})$.[4] Up to this point the above representation is an exact method for the determination of the intensity field. To simplify the problem an approximation is now made by truncating the series in equation (16.1) after very few terms. By doing so, we have replaced the single unknown I (which is a function of space and direction) by

[2]The reader only interested in the P_1-approximation may skip directly to Section 16.5 after reading Section 16.2.

[3]All relations in this chapter are valid on a spectral basis and, for a gray medium, also for total quantities. For notational simplicity we omit any subscript used to emphasize the spectral nature of quantities.

[4]Obviously, a thorough understanding of the method requires the reader to be familiar with the method of separation of variables and generalized Fourier series, as applied to the solution of linear partial differential equations.

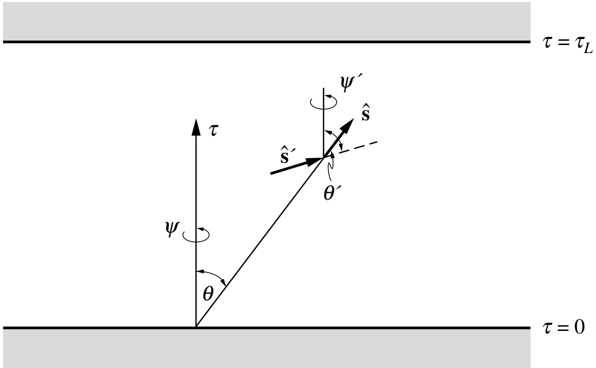

FIGURE 16-1
Coordinates for the one-dimensional plane-parallel medium.

$1 + 3 + \cdots + (2N + 1) = (N + 1)^2$ unknown I_l^m that are functions of space only. Therefore, we need to replace equation (16.4) (a function of space and direction) by $(N + 1)^2$ equations (which are functions of space only). This is achieved by multiplying equation (16.4) by Y_k^m and integrating over all directions.

The highest value for l retained, N, gives the method its order and its name. Most often employed is the P_1 or *differential approximation* ($l = 0, 1$), while the P_3-approximation ($l = 0, 1, 2, 3$) has been used a few times. It is known from neutron transport theory that approximations of odd order are more accurate than even ones of next highest order, so that the P_2 approximation is never used. In most early developments and applications the P_N-method was derived only for the one-dimensional plane-parallel case, for example, as in Jeans [1], Kourganoff [2], and Krook [7]. Detailed derivations of the general three-dimensional case in Cartesian coordinates have been given by Davison [3] and by Cheng [8,9]. The extension to general coordinate systems has been given by Ou and Liou [10]. Another general three-dimensional derivation has been given by Condiff [11], who expanded the intensity in terms of *polyadic Legendre polynomials* given by Brenner [12], that is, Legendre functions $P_n(\hat{\mathbf{s}})$ whose arguments are tensors of order n (rather than scalars). And, recently, Modest and Yang [13], have formulated the general three-dimensional P_N-approximation for Cartesian geometries in terms of elliptic second-order partial differential equations, which are readily incorporated into standard CFD codes.

16.3 THE P_N-APPROXIMATION FOR A ONE-DIMENSIONAL SLAB

We shall now develop the general P_N-method in some detail for the one-dimensional plane-parallel medium, in order to (*i*) shed further light on the general method, and (*ii*) facilitate the difficult problem of developing a consistent set of boundary conditions. For such a simple case the intensity does not depend on azimuthal angle ψ (assuming the polar angle θ is measured from an axis perpendicular to the plates, as shown in Fig. 16-1), i.e., $I_l^m = 0$ for $m \neq 0$. Thus, equation (16.1) may be simplified to

$$I(\tau, \mu) \simeq \sum_{l=0}^{N} I_l(\tau) P_l(\mu), \tag{16.5}$$

where we set $\mu = \cos\theta$ and omitted the superscript "0" from I_l since it is no longer necessary. Equation (16.5) is approximate because the series is truncated beyond $l = N$, i.e., we assume $I_l(\tau) = 0$ for all $l > N$. The scattering phase function for such a medium, expanded into Legendre polynomials, is [see equation (14.12)]

$$\Phi(\mu, \mu') = \sum_{m=0}^{M} A_m P_m(\mu') P_m(\mu), \tag{16.6}$$

where M is the order of approximation for the phase function; and we find

$$\int_{-1}^{1} \Phi(\mu,\mu')I(\tau,\mu')\,d\mu' = \sum_{l=0}^{N} I_l(\tau)\sum_{m=0}^{M} A_m P_m(\mu)\int_{-1}^{1} P_l(\mu')P_m(\mu')\,d\mu'. \tag{16.7}$$

We may now utilize the orthogonality of Legendre polynomials (see, for example, Abramowitz and Stegun [14]), to write

$$\int_{-1}^{1} P_l(\mu)P_m(\mu)\,d\mu = \frac{2\delta_{lm}}{2m+1} = \begin{cases} 0 & \text{for } m \neq l, \\ \dfrac{2}{2m+1} & \text{for } m = l. \end{cases} \tag{16.8}$$

Employing this orthogonality relation in equation (16.7) leads to

$$\int_{-1}^{1} \Phi(\mu,\mu')I(\tau,\mu')\,d\mu' = \sum_{l=0}^{N} \frac{2A_l}{2l+1} I_l(\tau)P_l(\mu), \tag{16.9}$$

where it is implied that $A_l = 0$ for $l > M$. (On the other hand, if $M > N$, the A_l for $l = N+1,\ldots,M$ disappear and this information about the phase function is lost in the Nth order approximation.) We may now recast the equation of transfer for the one-dimensional plane-parallel medium as

$$\mu\frac{dI}{d\tau} + I(\tau) = (1-\omega)I_b(\tau) + \frac{\omega}{2}\int_{-1}^{1} \Phi(\mu,\mu')I(\tau,\mu')\,d\mu', \tag{16.10}$$

or

$$\sum_{l=0}^{N}\left[\frac{dI_l}{d\tau}\mu P_l(\mu) + I_l(\tau)P_l(\mu)\right] = (1-\omega)I_b(\tau) + \omega\sum_{l=0}^{N}\frac{A_l I_l(\tau)}{2l+1}P_l(\mu). \tag{16.11}$$

To exploit the orthogonality of the Legendre polynomials, we shall use the recursion relation [14]

$$(2l+1)\mu P_l(\mu) = lP_{l-1}(\mu) + (l+1)P_{l+1}(\mu). \tag{16.12}$$

Thus, we may recast equation (16.11) as

$$\sum_{l=0}^{N}\left\{\frac{I_l'(\tau)}{2l+1}\left[lP_{l-1}(\mu) + (l+1)P_{l+1}(\mu)\right] + I_l(\tau)P_l(\mu)\right\} = (1-\omega)I_b(\tau) + \sum_{l=0}^{N}\frac{\omega A_l I_l(\tau)}{2l+1}P_l(\mu), \tag{16.13}$$

where the prime denotes differentiation with respect to τ. Since we have introduced $(N+1)$ new variables, $I_0, I_1, \ldots, I_N$, we need to convert equation (16.13) into $(N+1)$ equations independent of direction. Thus, multiplying by $P_k(\mu)$ $(k = 0, 1, \ldots, N)$ and integrating over all μ leads to

$$\begin{aligned}\frac{k+1}{2k+3}I_{k+1}'(\tau) + \frac{k}{2k-1}I_{k-1}'(\tau) + \left(1 - \frac{\omega A_k}{2k+1}\right)I_k(\tau) &= (1-\omega)I_b(\tau)\delta_{0k}, \\ k &= 0, 1, \ldots, N,\end{aligned} \tag{16.14}$$

where equation (16.8) has been utilized. Equation (16.14) is a set of $(N+1)$ simultaneous first-order ordinary differential equations for the unknown functions $I_0(\tau)$, $I_1(\tau), \ldots, I_N(\tau)$.[5] As such it requires a set of $(N+1)$ boundary conditions for its solution.

16.4 BOUNDARY CONDITIONS FOR THE P_N-METHOD

The equation of radiative transfer, equation (16.4), is a first-order partial differential equation in intensity, requiring a boundary condition of the type

$$I(\mathbf{r}=\mathbf{r}_w, \hat{\mathbf{s}}) = I_w(\mathbf{r}_w, \hat{\mathbf{s}}) \quad \text{for } \hat{\mathbf{n}}\cdot\hat{\mathbf{s}} > 0 \tag{16.15}$$

[5] Remember that equation (16.5) is truncated beyond $l = N$, so that $I_{N+1}(\tau) = 0$.

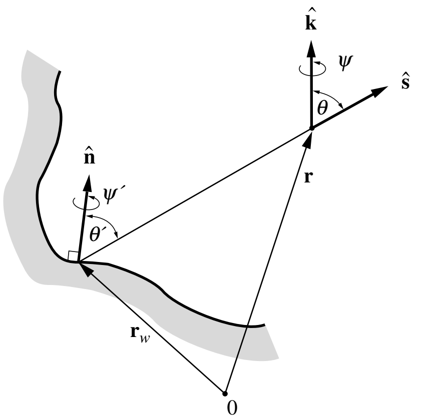

FIGURE 16-2
Prescribed boundary intensities for P_N-method.

everywhere on the surface, that is, the intensity leaving a surface (described by the vector $\mathbf{r}_w$) must be prescribed in some fashion for all outgoing directions $\hat{\mathbf{n}}\cdot\hat{\mathbf{s}} > 0$ (with $\hat{\mathbf{n}}$ being the outward surface normal), as shown in Fig. 16-2.

When the P_N-approximation is applied [truncating equation (16.1) after $l = N$] this boundary condition can no longer be satisfied and must be replaced by one that either satisfies equation (16.15) at selected directions $\hat{\mathbf{s}}_i$ or satisfies it in an integral sense. Mark [15, 16] and Marshak [17] proposed two different sets of boundary conditions for the spherical harmonics method as applied to neutron transport within a one-dimensional plane-parallel medium.

Mark's Boundary Condition

For a one-dimensional slab of optical thickness τ_L, equation (16.15) may be rewritten as

$$I(0,\mu) = I_{w1}(\mu), \qquad 0 < \mu < 1, \tag{16.16a}$$

$$I(\tau_L,\mu) = I_{w2}(\mu), \qquad -1 < \mu < 0, \tag{16.16b}$$

where I_{w1} and I_{w2} are the prescribed intensities at Surfaces 1 ($\tau = 0$) and 2 ($\tau = \tau_L$).[6]

The P_N-method for such a medium, equation (16.14), requires $(N + 1)$ boundary conditions, say $\frac{1}{2}(N + 1)$ each, at $\tau = 0$ and $\tau = \tau_L$ (assuming that N is odd). Noting that the equation

$$P_{N+1}(\mu) = 0 \tag{16.17}$$

has precisely $\frac{1}{2}(N + 1)$ roots μ_i with values between 0 and 1, Mark suggested replacing the boundary conditions of equation (16.16) by

$$I(0,\mu = \mu_i) = I_{w1}(\mu_i), \qquad i = 1, 2, \ldots, \tfrac{1}{2}(N + 1), \tag{16.18a}$$

$$I(\tau_L,\mu = -\mu_i) = I_{w2}(-\mu_i), \qquad i = 1, 2, \ldots, \tfrac{1}{2}(N + 1), \tag{16.18b}$$

where the μ_i are the positive roots of equation (16.17). A detailed explanation for this choice has been given by Mark [15, 16] and by Davison [3]. For example, for the P_1-approximation for a medium bounded by black walls we get with $P_2(\mu) = \frac{1}{2}(3\mu^2 - 1)$, $\mu_1 = 1/\sqrt{3}$ and, from equation (16.5),

$$I\left(0,\mu = \frac{1}{\sqrt{3}}\right) = I_0(0) + \frac{I_1(0)}{\sqrt{3}} = I_{b1}, \tag{16.19a}$$

$$I\left(\tau_L,\mu = -\frac{1}{\sqrt{3}}\right) = I_0(\tau_L) - \frac{I_1(\tau_L)}{\sqrt{3}} = I_{b2}. \tag{16.19b}$$

[6]We include the subscript w here to distinguish the I_{wi} from the intensity moments I_i defined by equation (16.5).

One serious drawback of Mark's boundary conditions is the fact that they are difficult, if not impossible, to apply to more complicated geometries.

Marshak's Boundary Conditions

An alternative set of boundary conditions for the one-dimensional plane-parallel P_N-approximation was proposed by Marshak, who suggested that equation (16.16) be satisfied in an integral sense by setting

$$\int_0^1 I(0,\mu)P_{2i-1}(\mu)\,d\mu = \int_0^1 I_{w1}(\mu)P_{2i-1}(\mu)\,d\mu, \qquad i=1,2,\ldots,\tfrac{1}{2}(N+1); \tag{16.20a}$$

$$\int_{-1}^0 I(\tau_L,\mu)P_{2i-1}(\mu)\,d\mu = \int_{-1}^0 I_{w2}(\mu)P_{2i-1}(\mu)\,d\mu, \qquad i=1,2,\ldots,\tfrac{1}{2}(N+1). \tag{16.20b}$$

Again, the reason for choosing all the Legendre polynomials of odd order has been explained in detail by Marshak [17] and Davison [3]. Substituting equation (16.5) and assuming diffuse surfaces, i.e., $I_w = J_w/\pi$, leads to

$$\sum_{l=0}^{N} I_l(0)\int_0^1 P_l(\mu)P_{2i-1}(\mu)\,d\mu = \frac{J_{w1}}{\pi}\int_0^1 P_{2i-1}(\mu)\,d\mu, \qquad i=1,2,\ldots,\tfrac{1}{2}(N+1); \tag{16.21a}$$

$$\sum_{l=0}^{N} I_l(\tau_L)\int_{-1}^0 P_l(\mu)P_{2i-1}(\mu)\,d\mu = \frac{J_{w2}}{\pi}\int_{-1}^0 P_{2i-1}(\mu)\,d\mu, \qquad i=1,2,\ldots,\tfrac{1}{2}(N+1). \tag{16.21b}$$

As an example we again consider the P_1-approximation for a medium bounded by black walls. Then, with $P_1(\mu)=\mu$,

$$\int_0^1 I(0,\mu)\mu\,d\mu = \int_0^1 \left[I_0(0)+I_1(0)\mu\right]\mu\,d\mu = \int_0^1 I_{b1}\mu\,d\mu,$$

or

$$I_0(0)+\tfrac{2}{3}I_1(0) = I_{b1}, \tag{16.22a}$$

$$I_0(\tau_L)-\tfrac{2}{3}I_1(\tau_L) = I_{b2}. \tag{16.22b}$$

We note that replacing the factor 2 in Marshak's boundary condition by a $\sqrt{3}$ converts it to Mark's boundary condition.

One advantage of Marshak's boundary condition is that it may be extended to more general problems, although not painlessly. Note that the integration in equation (16.20) is carried out over all directions above the surface (i.e., a hemisphere) with the Legendre polynomials of equation (16.5) as weight factors. Thus, it appears natural to generalize the boundary condition to (see Fig. 16-2)

$$\int_{\hat{\mathbf{n}}\cdot\hat{\mathbf{s}}>0} I(\mathbf{r}_w,\hat{\mathbf{s}})\overline{Y}_{2i-1}^{m}(\hat{\mathbf{s}})\,d\Omega = \int_{\hat{\mathbf{n}}\cdot\hat{\mathbf{s}}>0} I_w(\hat{\mathbf{s}})\overline{Y}_{2i-1}^{m}(\hat{\mathbf{s}})\,d\Omega,$$
$$i=1,2,\ldots,\tfrac{1}{2}(N+1), \quad \text{all relevant } m, \tag{16.23}$$

where the $\overline{Y}_{2i-1}^{m}(\hat{\mathbf{s}})$ are expressed in terms of a local coordinate system, in which polar angle θ' is measured from the surface normal (i.e., $\cos\theta' = \hat{\mathbf{n}}\cdot\hat{\mathbf{s}}$), and azimuthal angle ψ' is measured on the surface, as indicated in Fig. 16-2. The statement "all relevant m" rather than $-i \le m \le +i$ appears in equation (16.23) since it may provide more boundary conditions than are required. For example, for a one-dimensional plane-parallel medium there is no azimuthal dependence,

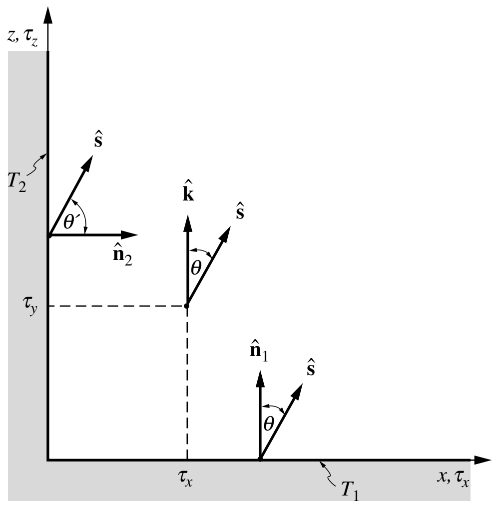

FIGURE 16-3
Geometry for Example 16.1.

so that all I_n^m with $m \neq 0$ vanish. and the only "relevant" value for m is $m = 0$. This leads to a single boundary condition on each surface for the P_1-approximation (as already seen to be correct), two for the P_3-approximation, and so on. Generally, equation (16.23) leads to too many boundary conditions in multidimensional situations. For example, for the P_1-approximation for a general three-dimensional medium without symmetry, equation (16.23) leads to three boundary conditions everywhere ($i = 1, m = 0, \pm 1$), while only one is needed (as explained in the following section). Davison [3] has shown that the number of superfluous conditions is always at least one less than the possible m at $i = \frac{1}{2}(N+1)$. Thus, on intuitive grounds it was accepted practice to satisfy equation (16.23) for all m for $i = 1, 2, \ldots, \frac{1}{2}(N-1)$, and for as many relevant m as possible for $i = \frac{1}{2}(N+1)$. Recently, Modest [18] has shown that a self-consistent set of boundary conditions is obtained if, for $i = \frac{1}{2}(N+1)$, only the even values for m are chosen, discarding all odd m.

Example 16.1. Consider the infinite quarter-space $\tau_x > 0, \tau_z > 0$ bounded by isothermal black surfaces at T_1 and T_2 as shown in Fig. 16-3. Develop the boundary conditions for the P_1-approximation at both surfaces (i.e., $\tau_x = 0$ and $\tau_z = 0$).

Solution
For the P_1-approximation equation (16.1) reduces to

$$I(\tau_x,\tau_z,\theta,\psi) = I_0^0(\tau_x,\tau_z) - I_1^{-1}(\tau_x,\tau_z)\sin\psi P_1^{-1}(\cos\theta) + I_1^0(\tau_x,\tau_z)P_1^0(\cos\theta) + I_1^1(\tau_x,\tau_z)\cos\psi P_1^1(\cos\theta).$$

For this two-dimensional problem it is convenient to measure polar angle θ from the τ_z-axis, and azimuthal angle ψ in the τ_x-τ_y-plane from the τ_x-axis. Then $I(\psi) = I(-\psi)$ and, with $P_1^0(\cos\theta) = \cos\theta$, and $P_1^1 = P_1^{-1}(\cos\theta) = -\sin\theta$,

$$I(\tau_x, \tau_y, \theta, \psi) = I_0^0 + I_1^0 \cos\theta - I_1^1 \cos\psi \sin\theta,$$

since the term involving $\sin\psi$ must vanish owing to symmetry. Therefore, equation (16.23) is able to provide two boundary conditions everywhere on the surface ($i = 1$ and $m = 0, 1$), while we need only one (as to be developed in the next section). Thus, following the discussion of equation (16.23), we introduce local direction coordinate systems on the surfaces and satisfy equation (16.23) only for $m = 0$. For the bottom surface, $\tau_z = 0$, the problem is simple since the surface normal is parallel to the τ_z-axis, from which the polar angle is measured. Thus,

$$\int_{\psi=0}^{2\pi}\int_{\theta=0}^{\pi/2}\left(I_0^0 + I_1^0\cos\theta - I_1^1\cos\psi\sin\theta\right)\cos\theta\sin\theta\,d\theta\,d\psi = \int_0^{2\pi}\int_0^{\pi/2} I_{b1}\cos\theta\sin\theta\,d\theta\,d\psi,$$

or

$$I_0^0(\tau_x, 0) + \tfrac{2}{3} I_1^0(\tau_x, 0) = I_{b1}.$$

At the vertical surface ($\tau_x = 0$) $P_1^0 = \cos\theta'$, where θ' is the angle between a direction vector and the surface normal $\hat{\mathbf{n}} = \hat{\mathbf{\imath}}$. Thus, with $\cos\theta' = \hat{\mathbf{s}} \cdot \hat{\mathbf{\imath}}$ and $\hat{\mathbf{s}} = \sin\theta(\cos\psi\hat{\mathbf{\imath}} + \sin\psi\hat{\mathbf{\jmath}}) + \cos\theta\hat{\mathbf{k}}$, it follows that $\cos\theta' = \sin\theta\cos\psi$ and

$$\int_{\psi=-\pi/2}^{\pi/2} \int_{\theta=0}^{\pi} \left(I_0^0 + I_1^0 \cos\theta - I_1^1 \cos\psi \sin\theta\right) \sin\theta\cos\psi \sin\theta \, d\theta \, d\psi = \pi\left(I_0^0 - \tfrac{2}{3} I_1^1\right) = \pi I_{b2},$$

or

$$I_0^0(0, \tau_z) - \tfrac{2}{3} I_1^1(0, \tau_z) = I_{b2}.$$

We shall see in the next section that I_0^0 is directly proportional to incident radiation, while I_1^0 and I_1^1 are proportional to radiative heat flux into the τ_y- and τ_x-directions, respectively.

Davison [3] stated that for low-order approximations Marshak's boundary conditions would give superior results, but that for high-order approximations Mark's boundary conditions should be more accurate. However, subsequent numerical work by Pellaud [19] and Schmidt and Gelbard [20] showed Marshak's boundary condition leads to more accurate results, even in high-order approximations.

16.5 THE P_1-APPROXIMATION

If the series in equation (16.1) is truncated beyond $l = 1$ (i.e., $I_l^m \equiv 0$ for $l \geq 2$), we get the lowest-order, or P_1, approximation, or

$$I(\mathbf{r}, \hat{\mathbf{s}}) = I_0^0 Y_0^0 + I_1^{-1} Y_1^{-1} + I_1^0 Y_1^0 + I_1^1 Y_1^1. \tag{16.24}$$

From standard mathematical texts, such as MacRobert [21], or directly from equation (16.3) we find the associated Legendre polynomials as $P_0^0 = 1, P_1^0 = \cos\theta, P_1^1 = P_1^{-1} = -\sin\theta$, and, using equation (16.2),

$$I(\mathbf{r}, \theta, \psi) = I_0^0 + I_1^0 \cos\theta - I_1^{-1} \sin\theta \sin\psi - I_1^1 \sin\theta\cos\psi. \tag{16.25}$$

We notice that equation (16.25) has four terms: The first term is independent of direction, the second is proportional to the z-component of the direction vector $\hat{\mathbf{s}} = \sin\theta\cos\psi\hat{\mathbf{\imath}} + \sin\theta\sin\psi\hat{\mathbf{\jmath}} + \cos\theta\hat{\mathbf{k}}$, the third is proportional to s_y and the last to s_x.[7] Each term is preceded by an unknown function of the space coordinates, which are to be determined. Equation (16.25) may be written more compactly by introducing two new functions, a (a scalar) and $\mathbf{b}$ (a vector having three components) as

$$I(\mathbf{r}, \hat{\mathbf{s}}) = a(\mathbf{r}) + \mathbf{b}(\mathbf{r}) \cdot \hat{\mathbf{s}}. \tag{16.26}$$

The four unknowns—a and the three components of $\mathbf{b}$, or the four components of I_n^m—can be related to physical quantities. Substituting equation (16.26) into the definition for incident radiation yields

$$G(\mathbf{r}) = \int_{4\pi} I(\mathbf{r}, \hat{\mathbf{s}}) \, d\Omega = a(\mathbf{r}) \int_{4\pi} d\Omega + \mathbf{b}(\mathbf{r}) \cdot \int_{4\pi} \hat{\mathbf{s}} \, d\Omega = 4\pi a(\mathbf{r}), \tag{16.27}$$

since

$$\int_{4\pi} \hat{\mathbf{s}} \, d\Omega = \int_0^{2\pi} \int_0^{\pi} \begin{pmatrix} \sin\theta\cos\psi \\ \sin\theta\sin\psi \\ \cos\theta \end{pmatrix} \sin\theta \, d\theta \, d\psi = \begin{pmatrix} 0 \\ 0 \\ 0 \end{pmatrix} = \mathbf{0}. \tag{16.28}$$

[7] Provided the polar angle is measured from the z-axis, and the azimuthal angle from the x-axis.

Similarly, substituting equation (16.26) into the definition for the radiative heat flux gives

$$\mathbf{q}(\mathbf{r}) = \int_{4\pi} I(\mathbf{r},\hat{\mathbf{s}})\,\hat{\mathbf{s}}\,d\Omega = a(\mathbf{r})\int_{4\pi}\hat{\mathbf{s}}\,d\Omega + \mathbf{b}(\mathbf{r})\cdot\int_{4\pi}\hat{\mathbf{s}}\hat{\mathbf{s}}\,d\Omega = \frac{4\pi}{3}\mathbf{b}(\mathbf{r}), \tag{16.29}$$

since

$$\begin{aligned}
\int_{4\pi}\hat{\mathbf{s}}\hat{\mathbf{s}}\,d\Omega &= \int_0^{2\pi}\int_0^{\pi}\begin{pmatrix} \sin^2\theta\cos^2\psi & \sin^2\theta\sin\psi\cos\psi & \sin\theta\cos\theta\cos\psi \\ \sin^2\theta\sin\psi\cos\psi & \sin^2\theta\sin^2\psi & \sin\theta\cos\theta\sin\psi \\ \sin\theta\cos\theta\cos\psi & \sin\theta\cos\theta\sin\psi & \cos^2\theta \end{pmatrix}\times\sin\theta\,d\theta\,d\psi \\
&= \int_0^{\pi}\begin{pmatrix} \pi\sin^2\theta & 0 & 0 \\ 0 & \pi\sin^2\theta & 0 \\ 0 & 0 & 2\pi\cos^2\theta \end{pmatrix}\sin\theta\,d\theta \\
&= \frac{4\pi}{3}\begin{pmatrix} 1 & 0 & 0 \\ 0 & 1 & 0 \\ 0 & 0 & 1 \end{pmatrix} = \frac{4\pi}{3}\boldsymbol{\delta},
\end{aligned} \tag{16.30}$$

where $\boldsymbol{\delta}$ is the unit tensor, and $\mathbf{b}\cdot\boldsymbol{\delta} = \mathbf{b}$. Therefore, we may rewrite equation (16.26) in terms of incident radiation and radiative heat flux as

$$I(\mathbf{r},\hat{\mathbf{s}}) = \frac{1}{4\pi}[G(\mathbf{r}) + 3\mathbf{q}(\mathbf{r})\cdot\hat{\mathbf{s}}]. \tag{16.31}$$

We find that, except for a constant factor, I_0^0 is the incident radiation, while I_1^1, I_1^{-1}, and I_1^0 are the x-, y-, and z-components of the radiative heat flux, respectively. The preceding development is useful to show that equation (16.31) indeed corresponds to the lowest order of the P_N-approximation, equation (16.1). Of course, equation (16.31) should have physical significance and it should be possible to derive it from physical principles. This was done by Modest [22], who treated radiation as a "photon gas" with momentum and energy, and derived the intensity field through quantum statistics. He showed that the average photon velocity (which is proportional to heat flux) is inversely proportional to optical thickness, and that equation (16.31) holds for a location a large optical distance away from any points not at thermodynamic equilibrium (sharp temperature gradients, steps in temperature, etc.).

Now, substituting equation (16.31) into equation (16.4) and assuming linear-anisotropic scattering,[8]

$$\Phi(\hat{\mathbf{s}}\cdot\hat{\mathbf{s}}') = 1 + A_1\hat{\mathbf{s}}\cdot\hat{\mathbf{s}}', \tag{16.32}$$

leads to

$$\begin{aligned}
\int_{4\pi} I(\hat{\mathbf{s}}')\,\Phi(\hat{\mathbf{s}}\cdot\hat{\mathbf{s}}')\,d\Omega' &= \frac{1}{4\pi}\int_{4\pi}(G + 3\mathbf{q}\cdot\hat{\mathbf{s}}')(1 + A_1\hat{\mathbf{s}}\cdot\hat{\mathbf{s}}')\,d\Omega' \\
&= \frac{G}{4\pi}\left[\int_{4\pi} d\Omega' + A_1\hat{\mathbf{s}}\cdot\int_{4\pi}\hat{\mathbf{s}}'\,d\Omega'\right] + \frac{3\mathbf{q}}{4\pi}\cdot\left[\int_{4\pi}\hat{\mathbf{s}}'\,d\Omega' + A_1\left(\int_{4\pi}\hat{\mathbf{s}}'\hat{\mathbf{s}}'\,d\Omega'\right)\cdot\hat{\mathbf{s}}\right] \\
&= G + A_1\mathbf{q}\cdot\boldsymbol{\delta}\cdot\hat{\mathbf{s}} = G + A_1\mathbf{q}\cdot\hat{\mathbf{s}},
\end{aligned} \tag{16.33}$$

where equations (16.28) and (16.30) have been employed (and the last step is easily verified by, say, using Cartesian coordinates and carrying out the dot product). Thus, equation (16.4)

[8]Because of the orthogonality of spherical harmonics the P_1-approximation remains unchanged for nonlinear anisotropic scattering. The choice of the functional form for intensity, equation (16.31), does not allow such scattering behavior, i.e., the medium must be so optically thick that any nonlinear anisotropically scattered intensity is smoothed out in the immediate vicinity of the scattering point. In reality, this smoothing implies that a "best" linear-anisotropic scattering factor A_1^* must be determined.

becomes

$$\frac{1}{4\pi}\nabla_\tau\cdot[\hat{\mathbf{s}}(G+3\mathbf{q}\cdot\hat{\mathbf{s}})]+\frac{1}{4\pi}(G+3\mathbf{q}\cdot\hat{\mathbf{s}})\simeq(1-\omega)I_b+\frac{\omega}{4\pi}(G+A_1\mathbf{q}\cdot\hat{\mathbf{s}}),\tag{16.34}$$

where we were able to pull the direction vector $\hat{\mathbf{s}}$ inside the gradient, since direction is independent of position. Multiplying equation (16.34) by $Y_0^0=1$ and integrating over all solid angles gives

$$\nabla_\tau\cdot\mathbf{q}=(1-\omega)(4\pi I_b-G),\tag{16.35}$$

where again equations (16.28) and (16.30) have been invoked. Equation (16.35) is, of course, identical to equation (10.59) since it does not depend on the functional form for intensity.

To obtain additional equations we may multiply equation (16.34) by Y_1^m ($m=-1,0,+1$) or equivalently, by the components of the direction vector $\hat{\mathbf{s}}$. Choosing the latter and integrating over all directions leads to

$$\begin{aligned}\frac{1}{4\pi}\nabla_\tau\cdot\left[G\int_{4\pi}\hat{\mathbf{s}}\hat{\mathbf{s}}\,d\Omega+3\mathbf{q}\cdot\int_{4\pi}\hat{\mathbf{s}}\hat{\mathbf{s}}\hat{\mathbf{s}}\,d\Omega\right]+\frac{1}{4\pi}\left[G\int_{4\pi}\hat{\mathbf{s}}\,d\Omega+3\mathbf{q}\cdot\int_{4\pi}\hat{\mathbf{s}}\hat{\mathbf{s}}\,d\Omega\right]\\=(1-\omega)I_b\int_{4\pi}\hat{\mathbf{s}}\,d\Omega+\frac{\omega}{4\pi}\left[G\int_{4\pi}\hat{\mathbf{s}}\,d\Omega+A_1\mathbf{q}\cdot\int_{4\pi}\hat{\mathbf{s}}\hat{\mathbf{s}}\,d\Omega\right].\end{aligned}\tag{16.36}$$

It is easy to show that $\int_{4\pi}\hat{\mathbf{s}}\hat{\mathbf{s}}\hat{\mathbf{s}}\,d\Omega=0$ (and, indeed, the integral over any odd multiple of $\hat{\mathbf{s}}$) and, therefore, this equation reduces to

$$\frac{1}{3}\nabla_\tau\cdot(G\boldsymbol{\delta})+\mathbf{q}\cdot\boldsymbol{\delta}=\frac{\omega A_1}{3}\mathbf{q}\cdot\boldsymbol{\delta},$$

or

$$\nabla_\tau G=-(3-A_1\omega)\,\mathbf{q}.\tag{16.37}$$

Equations (16.35) and (16.37) are a complete set of one scalar and one vector equation in the unknowns G and $\mathbf{q}$, and are the governing equations for the P_1 or *differential approximation*. The heat flux may be eliminated from these equations by taking the divergence of equation (16.37) after dividing by $(1-A_1\omega/3)$:

$$\nabla_\tau\cdot\left(\frac{1}{1-A_1\omega/3}\nabla_\tau G\right)=-3\nabla_\tau\cdot\mathbf{q}=-3(1-\omega)(4\pi I_b-G).\tag{16.38}$$

If $A_1\omega$ is constant (does not vary across the volume) this equation reduces to

$$\nabla_\tau^2 G-(1-\omega)\,(3-A_1\omega)\,G=-(1-\omega)\,(3-A_1\omega)\,4\pi I_b.\tag{16.39}$$

Equation (16.39) is a *Helmholtz equation*, closely related to Laplace's equation, and is *elliptic* in nature (see, for example, a standard mathematics text such as Pipes and Harvill [23]). As such, it requires a single boundary condition specified everywhere on the enclosure surface.

If radiative equilibrium prevails, then $\nabla\cdot\mathbf{q}=0$, and

$$\nabla_\tau^2 G\;=\;0,\tag{16.40}$$

or

$$\nabla_\tau^2 I_b\;=\;0.\tag{16.41}$$

In either case we get the elliptic *Laplace's equation* with the same boundary condition requirements. Once the incident radiation and/or blackbody intensity has been determined, the radiative heat flux is found from equation (16.37) as

$$\mathbf{q}=-\frac{1}{3-A_1\omega}\nabla_\tau G.\tag{16.42}$$

Equation (16.23) can supply three boundary conditions for the P_1-approximation, while equations (16.39) or (16.40) only require a single one. Thus, following the discussion of Marshak's boundary condition, equation (16.23), we choose only the case of $m = 0$ for the weight function in equation (16.23), with polar angle measured from the surface normal. Thus,

$$\overline{Y}_1^0(\hat{\mathbf{s}}) = P_1^0(\cos\theta') = \cos\theta' = \hat{\mathbf{s}}\cdot\hat{\mathbf{n}}, \tag{16.43}$$

where θ' is the polar angle of $\hat{\mathbf{s}}$ in the local coordinate system as shown in Fig. 16-2. Physically, that is, without reference to the general P_N-approximation, this choice of boundary condition implies that the directional distribution of the outgoing intensity along the enclosure wall is satisfied in an integral sense, by requiring the normal heat flux to be continuous (from enclosure surface into the participating medium). Then the boundary condition becomes

$$\begin{aligned}\int_{\hat{\mathbf{n}}\cdot\hat{\mathbf{s}}>0} I_w(\hat{\mathbf{s}})\,\hat{\mathbf{s}}\cdot\hat{\mathbf{n}}\,d\Omega &= \frac{1}{4\pi}\int_{\hat{\mathbf{n}}\cdot\hat{\mathbf{s}}>0}(G+3\mathbf{q}\cdot\hat{\mathbf{s}})\,\hat{\mathbf{s}}\cdot\hat{\mathbf{n}}\,d\Omega\\ &= \frac{1}{4\pi}\int_{\psi'=0}^{2\pi}\int_{\theta'=0}^{\pi/2}\Big(G+3q_{t1}\sin\theta'\cos\psi'+3q_{t2}\sin\theta'\sin\psi'+3q_n\cos\theta'\Big)\cos\theta'\sin\theta'\,d\theta\,d\psi'\\ &= \frac{1}{2}\int_0^{\pi/2}(G+3q_n\cos\theta')\cos\theta'\sin\theta'\,d\theta' = \frac{1}{4}(G+2q_n)\end{aligned}$$

or

$$G + 2\mathbf{q}\cdot\hat{\mathbf{n}} = 4\int_{\hat{\mathbf{n}}\cdot\hat{\mathbf{s}}>0} I_w(\hat{\mathbf{s}})\,\hat{\mathbf{s}}\cdot\hat{\mathbf{n}}\,d\Omega. \tag{16.44}$$

Here q_{t1} and q_{t2} are the two components of the heat flux vector tangential to the surface and $q_n = \mathbf{q}\cdot\hat{\mathbf{n}}$ is the normal component.

For an opaque surface which emits and reflects radiation diffusely, $I_w(\hat{\mathbf{s}}) = J_w/\pi$, where J_w is the surface's radiosity. Substituting this into equation (16.44) leads to

$$G + 2\mathbf{q}\cdot\hat{\mathbf{n}} = \frac{4}{\pi}J_w\int_0^{2\pi}\int_0^{\pi/2}\cos\theta'\sin\theta'\,d\theta'\,d\psi' = 4J_w. \tag{16.45}$$

Recalling equation (5.26),

$$\mathbf{q}\cdot\hat{\mathbf{n}} = \frac{\epsilon}{1-\epsilon}\left(\pi I_{bw} - J_w\right), \tag{16.46}$$

equation (16.44) finally becomes

$$2\mathbf{q}\cdot\hat{\mathbf{n}} = 4J_w - G = \frac{\epsilon}{2-\epsilon}(4\pi I_{bw} - G), \tag{16.47}$$

where ϵ is the local surface emittance. Modest [22] has shown that equation (16.47) also holds if the surface reflectance consists of purely diffuse and purely specular components, i.e., if

$$\epsilon = 1 - \rho^d - \rho^s. \tag{16.48}$$

Thus, within the accuracy of the P_1, or differential, approximation, the results for enclosures with diffusely and/or specularly reflecting surfaces are identical. Since equation (16.39) is a second-order equation in G, it is of advantage to eliminate $\mathbf{q}\cdot\hat{\mathbf{n}}$ from the boundary condition using equation (16.42). Thus,

$$-\frac{2-\epsilon}{\epsilon}\frac{2}{3-A_1\omega}\hat{\mathbf{n}}\cdot\boldsymbol{\nabla}_\tau G + G = 4\pi I_{bw} \tag{16.49}$$

is the correct boundary condition to go with equation (16.38) or (16.39). Equation (16.49) is known as a *boundary condition of the third kind* (since it incorporates both the dependent variable and its normal gradient). Appendix F provides subroutine `P1sor` for the solution to this system for a two-dimensional (rectangular or axisymmetric-cylindrical) enclosure.

Summary of the P_1-Approximation

For convenience we will summarize here the pertinent equations and boundary conditions that constitute the P_1-approximation for a medium bounded by diffuse, gray walls. This can be done in two ways: *(i)* simultaneous first-order PDEs in incident radiation and radiative heat flux, or *(ii)* a single elliptic second-order PDE in incident radiation. The former is the preferred formulation for the case of radiative equilibrium in a gray medium; the latter is more useful if the temperature field is known (or must be found through iteration).

Simultaneous Equations:

$$\nabla \cdot \mathbf{q} = \kappa(4\pi I_b - G), \tag{16.50a}$$

$$\nabla G = -(3\beta - A_1\sigma_s)\,\mathbf{q}, \tag{16.50b}$$

$$\mathbf{r} = \mathbf{r}_w: \qquad 2\mathbf{q}\cdot\hat{\mathbf{n}} = 4J_w - G = \frac{\epsilon}{2-\epsilon}(4\pi I_{bw} - G). \tag{16.50c}$$

Incident Radiation Formulation:

$$\frac{1}{3\kappa}\nabla\cdot\left(\frac{1}{\beta - A_1\sigma_s/3}\nabla G\right) - G = -4\pi I_b, \tag{16.51a}$$

$$\mathbf{r} = \mathbf{r}_w: \qquad -\frac{2-\epsilon}{\epsilon}\,\frac{2}{3\beta - A_1\sigma_s}\hat{\mathbf{n}}\cdot\nabla G + G = 4\pi I_{bw}, \tag{16.51b}$$

and

$$\mathbf{q} = -\frac{1}{3\beta - A_1\sigma_s}\nabla G. \tag{16.52}$$

Example 16.2. Consider an isothermal, gray slab at temperature T and of optical thickness τ_L, bounded by two isothermal black surfaces at temperature T_w. The medium scatters linear-anisotropically. Determine an expression of the nondimensional heat flux as a function of the optical parameters.

Solution
Since the temperature field is given we use the incident radiation formulation, and we may write equation (16.39) or equation (16.51*a*) as

$$\frac{d^2G}{d\tau^2} - (1-\omega)(3 - A_1\omega)\,G = -(1-\omega)(3-A_1\omega)\,4n^2\sigma T^4,$$

or

$$G(\tau) = C_1\cosh\gamma\tau + C_2\sinh\gamma\tau + 4n^2\sigma T^4,$$

where

$$\gamma = \sqrt{(1-\omega)(3-A_1\omega)}.$$

Because of the symmetry of the problem it is advantageous to place the origin at the center of the slab, i.e., $-\tau_L/2 \leq \tau \leq +\tau_L/2$. Then

$$\frac{dG}{d\tau}(\tau=0) = 0 = \gamma C_1\sinh(\gamma\times 0) + \gamma C_2\cosh(\gamma\times 0) + 0,$$

or $C_2 = 0$. Applying equation (16.49) [or (16.51*b*)] at $\tau = \tau_L/2$, with $\epsilon = 1$, we get

$$\frac{2}{3-A_1\omega}\frac{dG}{d\tau}(\tau_L/2) + G(\tau_L/2) = 4n^2\sigma T_w^4,$$

or

$$\frac{2\gamma}{3-A_1\omega}C_1\sinh\tfrac{1}{2}\gamma\tau_L + C_1\cosh\tfrac{1}{2}\gamma\tau_L + 4n^2\sigma T^4 = 4n^2\sigma T_w^4,$$

$$C_1 = -\frac{4n^2\sigma(T^4 - T_w^4)}{\cosh\frac{1}{2}\gamma\tau_L + 2\sqrt{\frac{1-\omega}{3-A_1\omega}}\sinh\frac{1}{2}\gamma\tau_L},$$

and

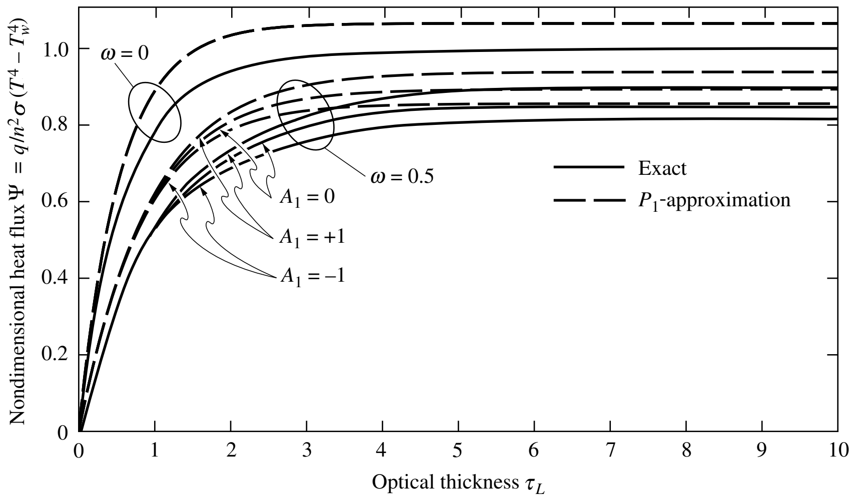

FIGURE 16-4
Nondimensional wall heat fluxes for a constant-temperature slab with linear-anisotropic scattering.

$$G(\tau) = 4n^2\sigma T^4 - 4n^2\sigma(T^4 - T_w^4)\frac{\cosh \gamma\tau}{\cosh \frac{1}{2}\gamma\tau_L + 2\sqrt{\frac{1-\omega}{3-A_1\omega}}\sinh \frac{1}{2}\gamma\tau_L}.$$

The heat flux is determined from equation (16.42) as

$$\Psi = \frac{q}{n^2\sigma(T^4 - T_w^4)} = -\frac{1}{n^2\sigma(T^4 - T_w^4)}\frac{1}{3 - A_1\omega}\frac{dG}{d\tau} = \frac{2\sinh \gamma\tau}{\sinh \frac{1}{2}\gamma\tau_L + \frac{1}{2}\sqrt{\frac{3-A_1\omega}{1-\omega}}\cosh \frac{1}{2}\gamma\tau_L}.$$

Some sample results for the heat flux at the wall ($\tau = \tau_L/2$) are given in Fig. 16-4. We note that in this case the P_1-approximation goes to the correct optically thin limit $\Psi \to 4\tau/\tau_L$ (emission, but no self-absorption of emission), but not to the correct optically thick limit (since, as a result of the temperature step at the wall, there will always be an intensity discontinuity at the wall). In fact, for this problem the results of the P_1-approximation are worst (in absolute magnitude) close to that location.

Example 16.3. Let us look at a gray medium at radiative equilibrium placed between two black concentric cylinders of radius R_1 and R_2 that are isothermal at temperatures T_1 and T_2. For simplicity, we shall assume that the medium does not scatter ($\sigma_s = 0$), and that its absorption coefficient, κ, is constant. We desire to find the heat flux from inner to outer cylinder as a function of the ratio R_1/R_2 and the optical thickness of the medium, $\tau_{12} = \tau_2 - \tau_1 = \kappa(R_2 - R_1)$.

Solution
For one-dimensional radiative equilibrium problems such as this, it is advantageous to use the simultaneous equation formulation, equations (16.50*a*) and (16.50*b*). Then, from equation (16.50*a*) we have, in cylindrical coordinates (with $\omega = 0$ and $\tau = \kappa r$),

$$\frac{1}{\tau}\frac{d}{d\tau}(\tau q) = 4n^2\sigma T^4 - G = 0.$$

If we multiply by τ and integrate, we find

$$\tau q = C_1 \quad \text{or} \quad q = \frac{C_1}{\tau}.$$

Substituting this expression into equation (16.37) gives

$$\frac{dG}{d\tau} = -3q = -\frac{3C_1}{\tau},$$

or

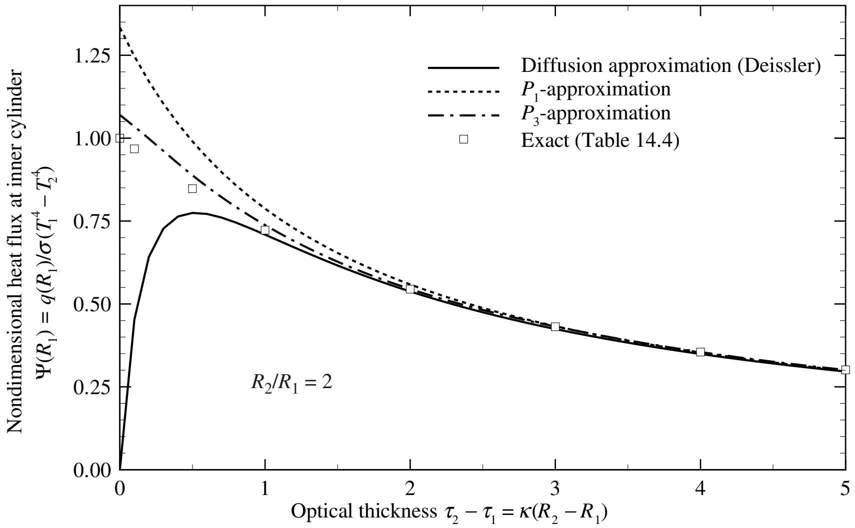

FIGURE 16-5
Nondimensional heat fluxes between concentric black cylinders at radiative equilibrium.

$$G = -3C_1 \ln \tau + C_2.$$

The boundary conditions are, from equation (16.47) with $\epsilon = 1$,

$$\tau = \tau_1 : \quad 2\mathbf{q} \cdot \hat{\mathbf{n}} = 2q = 4n^2\sigma T_1^4 - G,$$
$$\tau = \tau_2 : \quad 2\mathbf{q} \cdot \hat{\mathbf{n}} = -2q = 4n^2\sigma T_2^4 - G,$$

from which C_1 and C_2 may be determined as

$$C_1 = \frac{4n^2\sigma(T_1^4 - T_2^4)}{\dfrac{2}{\tau_1} + \dfrac{2}{\tau_2} + 3\ln\dfrac{\tau_2}{\tau_1}}, \quad C_2 = 4n^2\sigma T_2^4 + C_1\left(\frac{2}{\tau_2} + 3\ln\tau_2\right).$$

Heat flux and temperature then follow as

$$\Psi = \frac{q}{n^2\sigma\left(T_1^4 - T_2^4\right)} = \frac{2}{1 + \dfrac{\tau_2}{\tau_1} + \dfrac{3}{2}\tau_2 \ln\dfrac{\tau_2}{\tau_1}}\left(\frac{\tau_2}{\tau}\right),$$

$$\Phi = \frac{T^4 - T_2^4}{T_1^4 - T_2^4} = \frac{1 + \dfrac{3}{2}\tau_2 \ln\dfrac{\tau_2}{\tau}}{1 + \dfrac{\tau_2}{\tau_1} + \dfrac{3}{2}\tau_2 \ln\dfrac{\tau_2}{\tau_1}}.$$

The resulting nondimensional heat flux, Ψ, evaluated at the inner cylinder, is shown in Fig. 16-5 for the case of $R_2/R_1 = 2$ together with exact results (Table 14.4), results from the diffusion approximation with jump boundary condition (Example 15.3) and results from the P_3-approximation given by Bayazitoğlu and Higenyi [24]. As expected, the P_1-approximation does well for optically thick media. For the optically thin case, however, as $\kappa \to 0$ the heat flux goes to

$$\Psi_1 \to \frac{2}{1 + R_2/R_1}\frac{R_2}{R_1} = 2\Big/\left(1 + \frac{R_1}{R_2}\right),$$

while the correct answer should be $\Psi_1 \to 1$, as we know from Chapter 5, equation (5.35). Therefore, for $R_1/R_2 \to 1$ the correct optically thin limit is obtained (and the gap between such cylinders becomes a plane-parallel slab), while for small inner cylinders, $R_1/R_2 \ll 1$, the error becomes larger and may be as large as 100%!

The P_1-approximation is a very popular method since it reduces the (spectral or gray) equation of transfer from a very complicated integral equation to a relatively simple partial differential equation, e.g., [25–37]. The method is powerful (allowing nonblack surfaces, nonconstant properties, anisotropic scattering, etc.), and the average heat transfer engineer is much better trained in solving differential equations than integral equations. Furthermore, if overall energy conservation (also a partial differential equation) is computed, compatibility of the solution methods is virtually assured. However, it is important to remember that the P_1-approximation may be substantially in error in optically thin media with strongly anisotropic intensity distributions, in particular in multidimensional geometries with large aspect ratios (i.e., long and narrow configurations) and/or when surface emission dominates over medium emission. Attempts to improve the method's accuracy, by modifying Marshak's boundary condition, were made by Liu and coworkers [38] and by Su [39]. In one-dimensional geometries accuracy can also be improved by applying the P_1-approximation separately to different solid angle ranges, as done by Mengüç and Subramaniam [40]. Most of the shortcomings of the P_1-approximation are overcome by the *modified differential approximation* discussed in Section 16.8 below.

16.6 P_3- AND HIGHER-ORDER APPROXIMATIONS

The general P_N-approximation for one-dimensional absorbing/emitting, and anisotropically scattering cylindrical media has been given by Kofink [41], and the P_3-approximation for one-dimensional slabs, concentric cylinders, and concentric spheres has been developed in terms of moments by Bayazitoğlu and Higenyi [24]. Higher-order solutions, up to P_{11}, for a gray, anisotropically scattering medium between concentric spheres have been considered by Tong and Swathi [42] (uniform heat generation) and by Li and Tong [43] (isothermal medium). One-dimensional fibrous material was considered by Tong and Li [44] and a packed bed by Wu and Chu [45].

For multidimensional geometries, the process described in equations (16.11) through (16.14) can also be carried out in three dimensions, as outlined by Davison [3], resulting in a set of $(N+1)^2$ simultaneous, first-order partial differential equations in the unknown I_n^m. The general P_N-formulation for three-dimensional Cartesian coordinate systems has been derived by Cheng [8, 9], including Marshak's boundary conditions for surfaces normal to one of the coordinates. A three-dimensional problem was solved by Park and coworkers, analyzing radiative equilibrium in a rectangular box filled with a gray, nonscattering medium [26]. Mengüç and Viskanta [46, 47] limited their development to the P_3-approximation in terms of moments (rather than spherical harmonics), but considered three-dimensional Cartesian coordinates [46] as well as axisymmetric cylindrical geometries [47]. The three-dimensional P_N-approximation for arbitrary coordinate systems has been derived by Ou and Liou [10]. With the exception of Cheng [8], no boundary conditions beyond a reference to equation (16.23) have been given in these publications.

Recently, Modest and coworkers [13,18,48] outlined a methodology that reduces the $(N+1)^2$ simultaneous equations of the standard P_N-formulation to $N(N+1)/2$ simultaneous, second-order elliptic partial differential equations for a given odd order N, allowing for variable properties, anisotropic scattering, and arbitrary three-dimensional geometries. They further showed how to extract a completely defined, self-consistent set of boundary conditions from equation (16.23). The analysis is very tedious, to say the least, and we will present here only the final result for the (somewhat simpler) case of isotropic scattering. Defining a second-order operator

$$\mathscr{L}_{xy} = \frac{1}{\beta}\frac{\partial}{\partial x}\left(\frac{1}{\beta}\frac{\partial}{\partial y}\right), \tag{16.53}$$

etc., and eliminating spherical harmonics coefficients I_n^m of odd order n, leads to the following set of second-order PDEs:

TABLE 16.1
Elliptic P_N-approximation coefficients for isotropic scattering

	$k=1$	$k=2$	$k=3$
$a_k^{nm\ (a)}$	$\dfrac{1}{4(2n+5)(2n+3)}$	$-\dfrac{1}{2(2n+3)(2n-1)}$	$\dfrac{1}{4(2n-1)(2n-3)}$
$b_k^{nm\ (a)}$	$\dfrac{n+m+1}{2(2n+5)(2n+3)}$	$-\dfrac{2m-1}{2(2n+3)(2n-1)}$	$-\dfrac{n-m}{2(2n-1)(2n-3)}$
c_k^{nm}	$-\dfrac{\pi_2(n+m+1)}{2(2n+5)(2n+3)}$	$\dfrac{n^2+n-1+m^2}{(2n+3)(2n-1)}$	$-\dfrac{\pi_2(n-m-1)}{2(2n-1)(2n-3)}$
d_k^{nm}	$-\dfrac{\pi_3(n+m+1)}{2(2n+5)(2n+3)}$	$-\dfrac{(2m+1)(n+m+1)(n-m)}{2(2n+3)(2n-1)}$	$\dfrac{\pi_3(n-m-2)}{2(2n-1)(2n-3)}$
e_k^{nm}	$\dfrac{\pi_4(n+m+1)}{4(2n+5)(2n+3)}$	$-\dfrac{\pi_2(n+m+1)\pi_2(n-m-1)}{2(2n+3)(2n-1)}$	$\dfrac{\pi_4(n-m-3)}{4(2n-1)(2n-3)}$

$^{(a)}a_k^{nm}=0$ for $m\le 1$, $b_k^{nm}=0$ for $m=0$;

$$\pi_k(n)=\prod_{j=0}^{k-1}(n+j)$$

$Y_n^m:\ n=0,2,\ldots,N-1,\ 0\le m\le n:$

$$\begin{aligned}\sum_{k=1}^{3}\Big\{&(\mathscr{L}_{xx}-\mathscr{L}_{yy})\Big[(1+\delta_{m2})a_k^{nm}I_{n+4-2k}^{m-2}+\frac{\delta_{m1}}{2}c_k^{nm}I_{n+4-2k}^{m}+e_k^{nm}I_{n+4-2k}^{m+2}\Big]\\ &+(\mathscr{L}_{xz}+\mathscr{L}_{zx})\Big[(1+\delta_{m1})b_k^{nm}I_{n+4-2k}^{m-1}+d_k^{nm}I_{n+4-2k}^{m+1}\Big]\\ &+(\mathscr{L}_{xy}+\mathscr{L}_{yx})\Big[-(1-\delta_{m2})a_k^{nm}I_{n+4-2k}^{-(m-2)}+\frac{\delta_{m1}}{2}c_k^{nm}I_{n+4-2k}^{-m}+e_k^{nm}I_{n+4-2k}^{-(m+2)}\Big]\\ &+(\mathscr{L}_{yz}+\mathscr{L}_{zy})\Big[-(1-\delta_{m1})b_k^{nm}I_{n+4-2k}^{-(m-1)}+d_k^{nm}I_{n+4-2k}^{-(m+1)}\Big]\\ &+(\mathscr{L}_{xx}+\mathscr{L}_{yy}-2\mathscr{L}_{zz})c_k^{nm}I_{n+4-2k}^{m}\Big\}+\left[\mathscr{L}_{zz}-(1-\omega\delta_{0n})\right]I_n^m=-(1-\omega)I_b\delta_{0n}\end{aligned}\tag{16.54a}$$

and

$Y_n^{-m}:\ n=0,2,\ldots,N-1,\ 1\le m\le n:$

$$\begin{aligned}\sum_{k=1}^{3}\Big\{&(\mathscr{L}_{xy}+\mathscr{L}_{yx})\Big[(1+\delta_{m2})a_k^{nm}I_{n+4-2k}^{m-2}+\frac{\delta_{m1}}{2}c_k^{nm}I_{n+4-2k}^{m}-e_k^{nm}I_{n+4-2k}^{m+2}\Big]\\ &+(\mathscr{L}_{yz}+\mathscr{L}_{zy})\Big[(1+\delta_{m1})b_k^{nm}I_{n+4-2k}^{m-1}-d_k^{nm}I_{n+4-2k}^{m+1}\Big]\\ &+(\mathscr{L}_{xx}-\mathscr{L}_{yy})\Big[(1-\delta_{m2})a_k^{nm}I_{n+4-2k}^{-(m-2)}-\frac{\delta_{m1}}{2}c_k^{nm}I_{n+4-2k}^{-m}+e_k^{nm}I_{n+4-2k}^{-(m+2)}\Big]\\ &+(\mathscr{L}_{xz}+\mathscr{L}_{zx})\Big[(1-\delta_{m1})b_k^{nm}I_{n+4-2k}^{-(m-1)}+d_k^{nm}I_{n+4-2k}^{-(m+1)}\Big]\\ &+(\mathscr{L}_{xx}+\mathscr{L}_{yy}-2\mathscr{L}_{zz})c_k^{nm}I_{n+4-2k}^{-m}\Big\}+\left[\mathscr{L}_{zz}-1\right]I_n^{-m}=0.\end{aligned}\tag{16.54b}$$

The necessary constants[9] are listed in Table 16.1. For anisotropic scattering, not presented here,

[9]There is a slight error in the original paper [18], introducing a constant f_n, which after correction is $f_n\equiv 1$ and, thus, has been eliminated from equations (16.54).

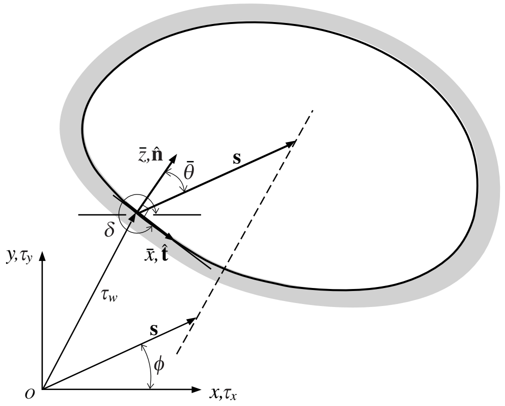

FIGURE 16-6
Local and global coordinates for a two-dimensional enclosure.

the constants for $k = 1$ and 3 undergo only minor changes, but for $k = 2$ [involving two different anisotropy constants A_m from equation (16.6)] the operators become nonsymmetric.

Since the orientation of the Cartesian coordinate system is arbitrary, one would expect to see equation (16.54) to show similar operators in x, y, and z. The reason that this is not the case is that the global direction angles (θ, ψ) and, thus, the results for I_n^m are tied to the choice of the coordinate system, i.e., we may write

$$I(\mathbf{r}, \hat{\mathbf{s}}) = \sum_{n}^{N} \sum_{m=-n}^{n} I_n^m(\mathbf{r}) Y_n^m(\hat{\mathbf{s}}) = \sum_{n}^{N} \sum_{m=-n}^{n} \overline{I}_n^m(\mathbf{r}) \overline{Y}_n^m(\hat{\mathbf{s}}), \tag{16.55}$$

where the barred values refer to a rotated coordinate system $(\overline{x}, \overline{y}, \overline{z})$.

Example 16.4. Consider an isothermal medium at temperature T, confined inside a two-dimensional enclosure as shown in Fig. 16-6. The medium is gray and absorbs and emits, but does not scatter. Determine the set of governing equations for the P_3-approximation.

Solution

For a two-dimensional problem with polar angle θ measured from the z-axis we must have $I(\theta, \psi) = I(\pi - \theta, \psi)$, i.e., all I_n^m, for which the accompanying associated Legendre polynomials $P_n^m(\cos\theta)$ have an odd-power dependence on $\cos\theta$, must vanish. This is the case whenever $n + m$ is odd. Therefore, $I_n^m = 0$ for $n + m =$ odd and, since the governing equations are cast in terms of even n, terms with odd m in equations (16.54) vanish. Using this, and eliminating all terms with z-derivatives, we get from equations (16.54)

$$\begin{aligned}
Y_0^0 &: (\mathscr{L}_{xx} - \mathscr{L}_{yy}) e_1^{00} I_2^2 + (\mathscr{L}_{xy} + \mathscr{L}_{yx}) e_1^{00} I_2^{-2} + (\mathscr{L}_{xx} + \mathscr{L}_{yy}) c_1^{00} I_2^0 + (\mathscr{L}_{xx} + \mathscr{L}_{yy}) c_2^{00} I_0^0 - I_0^0 = -I_b,\\
Y_2^0 &: (\mathscr{L}_{xx} - \mathscr{L}_{yy}) e_2^{20} I_2^2 + (\mathscr{L}_{xy} + \mathscr{L}_{yx}) e_2^{20} I_2^{-2} + (\mathscr{L}_{xx} + \mathscr{L}_{yy}) c_2^{20} I_2^0 + (\mathscr{L}_{xx} + \mathscr{L}_{yy}) c_3^{20} I_0^0 - I_2^0 = 0,\\
Y_2^2 &: (\mathscr{L}_{xx} - \mathscr{L}_{yy}) 2a_2^{22} I_2^0 + (\mathscr{L}_{xx} + \mathscr{L}_{yy}) c_2^{22} I_2^2 + (\mathscr{L}_{xx} - \mathscr{L}_{yy}) 2a_3^{22} I_0^0 \qquad - I_2^2 = 0,\\
Y_2^{-2} &: (\mathscr{L}_{xy} + \mathscr{L}_{yx}) 2a_2^{22} I_2^0 + (\mathscr{L}_{xx} + \mathscr{L}_{yy}) c_2^{22} I_2^{-2} + (\mathscr{L}_{xy} + \mathscr{L}_{yx}) 2a_3^{22} I_0^0 \qquad - I_0^{-2} = 0.
\end{aligned}$$

For $n = 0$ the case of $k = 3$ is not needed, since this leads to nonexistent I_{-2}^m, and, similarly, for $n = 2$ the case of $k = 1$, producing I_4^m, i.e., terms omitted in the P_3-approximation. In addition, all I_n^m with odd m and with $m > n$ are dropped. Equations (16.54) are also valid for $n = 2, m = \pm 1$, but every term in these equations vanishes. Thus the above set constitutes the needed four equations for the four unknowns. The coefficients are evaluated from Table 16.1 as

$$a_2^{22} = -\frac{1}{2 \cdot 7 \cdot 3} = -\frac{1}{42};\ a_3^{22} = \frac{1}{4 \cdot 3 \cdot 1} = \frac{1}{12};\ e_1^{00} = \frac{1 \cdot 2 \cdot 3 \cdot 4}{4 \cdot 5 \cdot 3} = \frac{2}{5};\ e_2^{20} = -\frac{3 \cdot 4 \cdot 1 \cdot 2}{2 \cdot 7 \cdot 3} = -\frac{4}{7};$$
$$c_1^{00} = -\frac{1 \cdot 2}{2 \cdot 5 \cdot 3} = -\frac{1}{15};\ c_2^{00} = \frac{-1}{3 \cdot (-1)} = \frac{1}{3};\ c_2^{20} = \frac{5}{7 \cdot 3} = \frac{5}{21};\ c_2^{22} = \frac{9}{7 \cdot 3} = \frac{3}{7};\ c_3^{20} = -\frac{1 \cdot 2}{2 \cdot 3 \cdot 1} = -\frac{1}{3}.$$

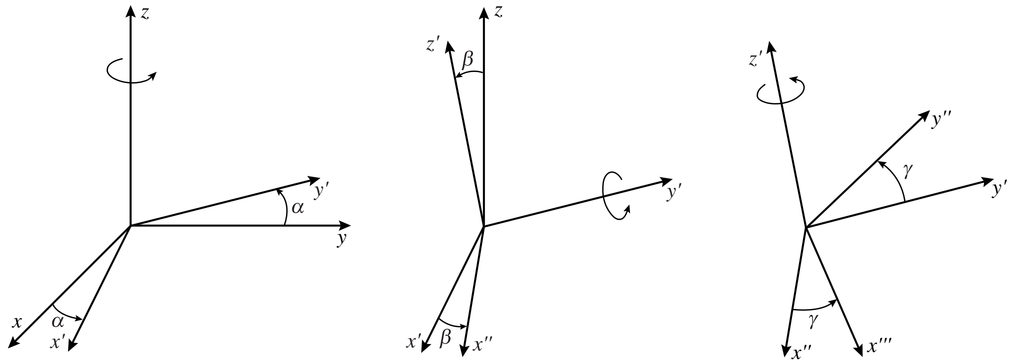

FIGURE 16-7
Definition of Euler angles for an arbitrary rotation

Substituting these values into the four governing equations, we find

$$Y_0^0: \quad \frac{2}{5}(\mathscr{L}_{xx} - \mathscr{L}_{yy})I_2^2 + \frac{2}{5}(\mathscr{L}_{xy} + \mathscr{L}_{yx})I_2^{-2} - (\mathscr{L}_{xx} + \mathscr{L}_{yy})\left(\frac{1}{15}I_2^0 - \frac{1}{3}I_0^0\right) - I_0^0 = -I_b, \tag{16.56a}$$

$$Y_2^0: \quad -\frac{4}{7}(\mathscr{L}_{xx} - \mathscr{L}_{yy})I_2^2 - \frac{4}{7}(\mathscr{L}_{xy} + \mathscr{L}_{yx})I_2^{-2} + (\mathscr{L}_{xx} + \mathscr{L}_{yy})\left(\frac{5}{21}I_2^0 - \frac{1}{3}I_0^0\right) - I_2^0 = 0, \tag{16.56b}$$

$$Y_2^2: \quad \frac{3}{7}(\mathscr{L}_{xx} + \mathscr{L}_{yy})I_2^2 - (\mathscr{L}_{xx} - \mathscr{L}_{yy})\left(\frac{1}{21}I_2^0 - \frac{1}{6}I_0^0\right) - I_2^2 = 0, \tag{16.56c}$$

$$Y_2^{-2}: \quad \frac{3}{7}(\mathscr{L}_{xx} + \mathscr{L}_{yy})I_2^{-2} - (\mathscr{L}_{xy} + \mathscr{L}_{yx})\left(\frac{1}{21}I_2^0 - \frac{1}{6}I_0^0\right) - I_2^{-2} = 0. \tag{16.56d}$$

Boundary Conditions

Equation set (16.54) consists of $N(N+1)/2$ simultaneous, elliptic PDEs, requiring $N(N+1)/2$ boundary conditions everywhere along the domain boundary, which must be determined from the general Marshak condition, equation (16.23). Unfortunately, equation (16.23) is cast in terms of a local coordinate system. Thus, in order to obtain a generic boundary condition for arbitrary geometries, the global spherical harmonics must be rotated into the local coordinate system. Such rotation, according to Euler's rotation theorem, may be described using three angles, which are called Euler angles. In the literature, there are several notation and rotation conventions for Euler angles. Here, the notation (α, β, γ) is used for three Euler angles following Varshalovich *et al.*'s definition [49]. In Varshalovich's convention, as shown in Fig. 16-7, an arbitrary rotation is defined by Euler angles (α, β, γ), where the first rotation is by an angle α about the z-axis, the second is by an angle β about the y'-axis, and the third is by an angle γ about the z'-axis. As indicated in Fig. 16-7 all three rotations are, following the right-hand rule, in counterclockwise direction about the center axis. The three rotations can, in general, be carried out by (1) rotating x-y so that y' is perpendicular to $\hat{\mathbf{n}}$ ($\hat{\mathbf{n}} \cdot \hat{\mathbf{j}}' = 0$),

$$\hat{\mathbf{i}}' = \cos\alpha\,\hat{\mathbf{i}} + \sin\alpha\,\hat{\mathbf{j}}, \quad \hat{\mathbf{j}}' = -\sin\alpha\,\hat{\mathbf{i}} + \cos\alpha\,\hat{\mathbf{j}} \tag{16.57}$$

and

$$\tan\alpha = \frac{n_y}{n_x}, \tag{16.58}$$

(2) rotating x'-z such that z' becomes parallel to $\hat{\mathbf{n}}$, or

$$\hat{\mathbf{k}}' = \sin\beta\,\hat{\mathbf{i}}' + \cos\beta\,\hat{\mathbf{k}} \tag{16.59}$$

and $\hat{\mathbf{n}} \cdot \hat{\mathbf{k}}' = 1$ gives

$$(n_x \cos\alpha + n_y \sin\alpha)\sin\beta + n_z \cos\beta = 1. \tag{16.60}$$

(3) The third rotation is arbitrary and serves to place the local $\overline{x}$-$\overline{y}$-coordinates into convenient locations.

Example 16.5. Determine the Euler angles for the local coordinate system for the boundary location indicated in Fig. 16-6.

Solution
To perform the transformation indicated in Fig. 16-6 (with the global z-axis pointing toward the reader), the local surface normal is determined as

$$\hat{\mathbf{n}} = -\sin\delta\,\hat{\imath} + \cos\delta\,\hat{\jmath} + 0\,\hat{\mathbf{k}}, \tag{16.61}$$

and the first rotation angle α follows from

$$\tan\alpha = -\tan\delta, \text{ or } \alpha = \delta \pm \frac{\pi}{2}. \tag{16.62}$$

If we choose $\alpha = \delta - \pi/2$ (y' points into the indicated $\overline{x}$-direction), the second rotation angle becomes

$$\left[-\sin\delta\cos\left(\delta - \frac{\pi}{2}\right) + \cos\delta\sin\left(\delta - \frac{\pi}{2}\right)\right]\sin\beta = 1, \text{ or } \beta = \frac{3\pi}{2}. \tag{16.63}$$

This has x'' pointing out of the paper, and a final (optional) rotation of $\gamma = \pi/2$ rotates x''' into the desired local $\overline{x}$-direction.

It can be shown that, for a given rotation, the spherical harmonics of order n are transformed into a linear combination of spherical harmonics of the same order n. Such an operation can be represented in the form of a rotation matrix, where each element of this matrix is a function of Euler angles,

$$Y_n^{m'}(\theta,\phi) = \sum_{m=-n}^{n} \Delta^n_{mm'}(\alpha,\beta,\gamma)\overline{Y}_n^m(\overline{\theta},\overline{\phi}), \tag{16.64}$$

where $\Delta^n_{mm'}(\alpha,\beta,\gamma)$ is the representation matrix of the rotation operation for the real spherical harmonics Y_n^m of order n. Blanco[10] *et al.* [50] developed a closed-form expression to specify all the elements based on so-called Wigner-D functions, from which the Δ^n matrices can be obtained in terms of the Euler angles as

$$\begin{aligned}\Delta^n_{mm'} &= \operatorname{sign}(m')\Psi_m(\alpha)\Psi_{m'}(\gamma)[d^n_{|m|,|m'|}(\beta) + (-1)^{m'} d^n_{|m|,-|m'|}(\beta)]\\ &\quad - \operatorname{sign}(m)\Psi_{-m}(\alpha)\Psi_{-m'}(\gamma)[d^n_{|m|,|m'|}(\beta) - (-1)^{m'} d^n_{|m|,-|m'|}(\beta)]\end{aligned} \tag{16.65}$$

where sign(0) = 1 and the function Ψ_m is defined as

$$\Psi_m(\xi) = \begin{cases} \cos m\xi, & \text{for} \quad m \geq 0,\\ \sin|m|\xi, & \text{for} \quad m < 0.\end{cases} \tag{16.66}$$

To determine the Δ^n matrices by equation (16.65) the d^n matrices are needed, which are modified versions of the real parts of the Wigner-$D^n_{mm'}$ functions, and may be calculated from

$$d^n_{mm'}(\beta) = \frac{(-1)^{m+m'}(n-|m|)!(n+|m'|)!}{1+\delta_{m,0}} \sum_{k=\max(0,m'-m)}^{\min(n-m,n+m')} \frac{(-1)^k\left(\cos\frac{\beta}{2}\right)^{2n-2k-m+m'}\left(\sin\frac{\beta}{2}\right)^{2k+m-m'}}{k!(n-m-k)!(n+m'-k)!(m-m'+k)!}. \tag{16.67}$$

With the rotation of spherical harmonics between local and global coordinates as indicated by equation (16.64), relationships between I_n^m and $\overline{I}_n^m$ can be revealed accordingly by expressing

[10]In Blanco's derivation, a normalization factor is employed. In order to be consistent with the real spherical harmonics used in the current study, a modification coefficient was included in the transformation.

intensity in terms of, both, local and global coordinates, as given by equation (16.55). This leads to

$$I_n^m = \sum_{m'=-n}^{n} \Delta_{mm'}^n(\alpha,\beta,\gamma)\overline{I}_n^{m'}, \text{ and } \overline{I}_n^m = \sum_{m'=-n}^{n} \bar{\Delta}_{mm'}^n(-\gamma,-\beta,-\alpha)I_n^{m'}, \tag{16.68}$$

where the bar on the $\bar{\Delta}_{mm'}^n$ implies backward rotation from local to global coordinates, as indicated by the arguments. Substitution of equation (16.55) into (16.23), and assuming the surface intensity I_w to be diffuse, reduces the boundary conditions to

$$\sum_{n=0}^{N}\left[\int_0^1 P_n^m(\bar{\mu})P_{2i-1}^m(\bar{\mu})d\bar{\mu}\right]\overline{I}_n^m(\tau_w) = \left[\int_0^1 P_{2i-1}(\bar{\mu})d\bar{\mu}\right]\delta_{m,0}\, I_w,$$
$$i = 1,2,\ldots,\tfrac{1}{2}(N+1), \text{all relevant } m. \tag{16.69}$$

Before these boundary conditions can be applied to equations (16.54) the $\overline{I}_n^m$ with odd n must be eliminated. Boundary conditions are usually formulated in terms of local normal and tangential gradients, and this leads to

$$\begin{aligned}
\overline{Y}_{2i-1}^0 :\ & \sum_{l=0}^{\frac{N-1}{2}} p_{2l,2i-1}^0 \overline{I}_{2l}^0 + \frac{\partial}{\partial\tau_{\overline{x}}}\left[\sum_{l=1}^{\frac{N-1}{2}} v_{li}^0 \overline{I}_{2l}^1\right] \\
& + \frac{\partial}{\partial\tau_{\overline{y}}}\left[\sum_{l=1}^{\frac{N-1}{2}} v_{li}^0 \overline{I}_{2l}^{-1}\right] - \frac{\partial}{\partial\tau_{\overline{z}}}\left[\sum_{l=0}^{\frac{N-1}{2}} w_{li}^0 \overline{I}_{2l}^0\right] = I_w p_{0,2i-1}^0, \qquad m=0, \qquad (16.70a)\\
\overline{Y}_{2i-1}^m :\ & \sum_{l=1}^{\frac{N-1}{2}} p_{2l,2i-1}^m \overline{I}_{2l}^m - \frac{\partial}{\partial\tau_{\overline{x}}}\left[\sum_{l=0}^{\frac{N-1}{2}} (1+\delta_{m,1})u_{li}^m \overline{I}_{2l}^{m-1} - \sum_{l=1}^{\frac{N-1}{2}} v_{li}^m \overline{I}_{2l}^{m+1}\right] \\
& + \frac{\partial}{\partial\tau_{\overline{y}}}\left[\sum_{l=1}^{\frac{N-1}{2}} (1-\delta_{m,1})u_{li}^m \overline{I}_{2l}^{-(m-1)} + \sum_{l=1}^{\frac{N-1}{2}} v_{li}^m \overline{I}_{2l}^{-(m+1)}\right] - \frac{\partial}{\partial\tau_{\overline{z}}}\left[\sum_{l=1}^{\frac{N-1}{2}} w_{li}^m \overline{I}_{2l}^m\right] = 0, \qquad m>0, \qquad (16.70b)\\
\overline{Y}_{2i-1}^{-m} :\ & \sum_{l=1}^{\frac{N-1}{2}} p_{2l,2i-1}^m \overline{I}_{2l}^{-m} - \frac{\partial}{\partial\tau_{\overline{x}}}\left[\sum_{l=1}^{\frac{N-1}{2}} (1-\delta_{m,1})u_{li}^m \overline{I}_{2l}^{-(m-1)} - \sum_{l=1}^{\frac{N-1}{2}} v_{li}^m \overline{I}_{2l}^{-(m+1)}\right] \\
& - \frac{\partial}{\partial\tau_{\overline{y}}}\left[\sum_{l=0}^{\frac{N-1}{2}} (1+\delta_{m,1})u_{li}^m \overline{I}_{2l}^{m-1} + \sum_{l=1}^{\frac{N-1}{2}} v_{li}^m \overline{I}_{2l}^{m+1}\right] - \frac{\partial}{\partial\tau_{\overline{z}}}\left[\sum_{l=1}^{\frac{N-1}{2}} w_{li}^m \overline{I}_{2l}^{-m}\right] = 0, \qquad m>0, \qquad (16.70c)
\end{aligned}$$

where the $p_{n,j}^m$ are defined as

$$p_{n,j}^m = p_{j,n}^m = \int_0^1 P_n^m(\bar{\mu})P_j^m(\bar{\mu})d\bar{\mu}, \tag{16.71}$$

and the coefficients $u_{li}^m, v_{li}^m, w_{li}^m$ are related to them by

$$u_{li}^m = \frac{p_{2l-1,2i-1}^m - p_{2l+1,2i-1}^m}{2(4l+1)}, \tag{16.72a}$$

$$v_{li}^m = \frac{\pi_2(2l+m)p_{2l-1,2i-1}^m - \pi_2(2l-m)p_{2l+1,2i-1}^m}{2(4l+1)}, \tag{16.72b}$$

$$w_{li}^m = \frac{(2l+m)p_{2l-1,2i-1}^m + (2l-m+1)p_{2l+1,2i-1}^m}{(4l+1)}. \tag{16.72c}$$

TABLE 16.2
Half-moments of associated Legendre polynomials, $10^{-m} \times p^m_{n,j}$.

m	$n\backslash j$	0	1	2	3	4	5
0	0	1.00000	.	.	.	.	.
	1	0.50000	0.33333	.	.	.	.
	2	0.00000	0.12500	0.20000	.	.	.
	3	–0.12500	0.00000	0.12500	0.14286	.	.
	4	0.00000	–0.02083	0.00000	0.07031	0.11111	.
	5	0.06250	0.00000	–0.03906	0.00000	0.07031	0.09091
1	1	.	0.06667	.	.	.	.
	2	.	0.07500	0.12000	.	.	.
	3	.	0.00000	0.07500	0.17143	.	.
	4	.	–0.04167	0.00000	0.14062	0.22222	.
	5	.	0.00000	–0.02344	0.00000	0.14062	0.27273
2	2	.	.	0.04800	.	.	.
	3	.	.	0.07500	0.17143	.	.
	4	.	.	0.00000	0.14062	0.40000	.
	5	.	.	–0.06563	0.00000	0.39375	0.76364
3	3	.	.	.	0.10286	.	.
	4	.	.	.	0.19687	0.56000	.
	5	.	.	.	0.00000	0.55125	1.83273
4	4	.	.	.	.	0.44800	.
	5	.	.	.	.	0.99225	3.29891
5	5	.	.	.	.	.	3.29891

In equations (16.70) and (16.72) it is implied that coefficients in front of nonsensical $\overline{I}^m_n$ (i.e., $|m| > n$) and p^m_{nj} with nonsensical subscripts ($n < m$) are zero. The $p^m_{n,j}$ may be determined through recursion relationships [18] and are listed in Table 16.2 (scaled by a factor of 10^{-m}) for up to the P_5-approximation.

It remains to rotate the $\overline{I}^m_n$ in equations (16.70) to global values I^m_n, which results in

$$\begin{aligned}
\overline{Y}^0_{2i-1}:\ & \sum_{l=0}^{\frac{N-1}{2}} \sum_{m'=-2l}^{2l} p^0_{2l,2i-1} \bar{\Delta}^{2l}_{0,m'} I^{m'}_{2l} + \frac{\partial}{\partial \tau_{\overline{x}}} \left\{ \sum_{l=1}^{\frac{N-1}{2}} \sum_{m'=-2l}^{2l} v^0_{li} \bar{\Delta}^{2l}_{1,m'} I^{m'}_{2l} \right\} \\
& + \frac{\partial}{\partial \tau_{\overline{y}}} \left\{ \sum_{l=1}^{\frac{N-1}{2}} \sum_{m'=-2l}^{2l} v^0_{li} \bar{\Delta}^{2l}_{-1,m'} I^{m'}_{2l} \right\} - \frac{\partial}{\partial \tau_{\overline{z}}} \left\{ \sum_{l=0}^{\frac{N-1}{2}} \sum_{m'=-2l}^{2l} w^0_{li} \bar{\Delta}^{2l}_{0,m'} I^{m'}_{2l} \right\} = I_w p^0_{0,2i-1}, \quad m = 0, \quad (16.73a)
\end{aligned}$$

$$\begin{aligned}
\overline{Y}^m_{2i-1}:\ & \sum_{l=1}^{\frac{N-1}{2}} \sum_{m'=-2l}^{2l} p^m_{2l,2i-1} \bar{\Delta}^{2l}_{m,m'} I^{m'}_{2l} - \frac{\partial}{\partial \tau_{\overline{x}}} \left\{ \sum_{l=0}^{\frac{N-1}{2}} \sum_{m'=-2l}^{2l} \left[(1+\delta_{m,1}) u^m_{li} \bar{\Delta}^{2l}_{m-1,m'} - v^m_{li} \bar{\Delta}^{2l}_{m+1,m'} \right] I^{m'}_{2l} \right\} \\
& + \frac{\partial}{\partial \tau_{\overline{y}}} \left\{ \sum_{l=1}^{\frac{N-1}{2}} \sum_{m'=-2l}^{2l} \left[(1-\delta_{m,1}) u^m_{li} \bar{\Delta}^{2l}_{-(m-1),m'} + v^m_{li} \bar{\Delta}^{2l}_{-(m+1),m'} \right] I^{m'}_{2l} \right\} - \frac{\partial}{\partial \tau_{\overline{z}}} \left\{ \sum_{l=1}^{\frac{N-1}{2}} \sum_{m'=-2l}^{2l} w^m_{li} \bar{\Delta}^{2l}_{m,m'} I^{m'}_{2l} \right\} = 0, \\
& \qquad m > 0, \qquad (16.73b)
\end{aligned}$$

$$\begin{aligned}
\overline{Y}^{-m}_{2i-1}:\ & \sum_{l=1}^{\frac{N-1}{2}} \sum_{m'=-2l}^{2l} p^m_{2l,2i-1} \bar{\Delta}^{2l}_{-m,m'} I^{m'}_{2l} - \frac{\partial}{\partial \tau_{\overline{x}}} \left\{ \sum_{l=1}^{\frac{N-1}{2}} \sum_{m'=-2l}^{2l} \left[(1-\delta_{m,1}) u^m_{li} \bar{\Delta}^{2l}_{-(m-1),m'} - v^m_{li} \bar{\Delta}^{2l}_{-(m+1),m'} \right] I^{m'}_{2l} \right\} \\
& - \frac{\partial}{\partial \tau_{\overline{y}}} \left\{ \sum_{l=0}^{\frac{N-1}{2}} \sum_{m'=-2l}^{2l} \left[(1+\delta_{m,1}) u^m_{li} \bar{\Delta}^{2l}_{m-1,m'} + v^m_{li} \bar{\Delta}^{2l}_{m+1,m'} \right] I^{m'}_{2l} \right\} - \frac{\partial}{\partial \tau_{\overline{z}}} \left\{ \sum_{l=1}^{\frac{N-1}{2}} \sum_{m'=-2l}^{2l} w^m_{li} \bar{\Delta}^{2l}_{-m,m'} I^{m'}_{2l} \right\} = 0, \\
& \qquad m > 0. \qquad (16.73c)
\end{aligned}$$

Equations (16.73) are a set of $(N+2)(N+1)/2$ boundary conditions for $N(N+1)/2$ variables I_{2l}^m ($l = 0, 1, ..., (N-1)/2$; $m = -2l, ..., +2l$), containing normal as well as tangential derivatives, or $N + 1$ too many. Commercial PDE solvers generally allow for boundary conditions containing normal derivatives. In principle, i.e., if the coefficients in front of the I_{2l}^m inside the normal derivatives form a nonsingular matrix, linear combination of the boundary conditions leads to a set of "natural" boundary conditions for each variable, or

$$\frac{\partial I_{2l}^m}{\partial \tau_{\overline{z}}} = f\left(I_{2l'}^{m'}, \frac{\partial I_{2l'}^{m'}}{\partial \tau_{\overline{x}}}, \frac{\partial I_{2l'}^{m'}}{\partial \tau_{\overline{y}}}; l' = 0, ... \tfrac{1}{2}(N-1); m' = -2l', ..., +2l'\right),$$
$$l = 0, ..., \tfrac{1}{2}(N-1), m = -2l, ..., +2l, \tag{16.74}$$

which can be used with FlexPDE [51] and other commercial programs. Modest [18] has shown that such a nonsingular matrix can be found only if, for the largest value of $i = \frac{1}{2}(N+1)$, only the even values of m are employed (omitting the $N+1$ odd values). Therefore, the qualifier "all relevant m" in equations (16.69), (16.70), and (16.73) may be restated precisely as

$$\text{All relevant } m = \begin{cases} i = 1, 2, ..., \frac{1}{2}(N-1), & \text{all } m, \\ i = \frac{1}{2}(N+1), & \text{all even } m, \end{cases} \tag{16.75}$$

which supplies a consistent set of $N(N + 1)/2$ boundary conditions for an equal number of variables.

Other codes, such as PDE2D [52] or FDEM [53], use derivatives in global coordinates in the boundary conditions. In that case, the transformation to global I_n^m using equation (16.68) is carried out first, followed by elimination of odd orders. The resulting boundary conditions are given in [13].

Example 16.6. Determine the necessary boundary conditions for the problem of Example 16.4 for the surface location indicated in Fig. 16-6. The surface is black and at temperature T_w.

Solution

The boundary conditions are usually expressed in terms of local coordinates (i.e., in terms of gradients into the surface normal and tangential directions), either using local spherical harmonics $\overline{I}_n^m$, equation (16.70), followed by rotation to global spherical harmonics I_n^m, or by directly applying equation (16.73). We will follow the first track here. With local azimuthal angle $\overline{\psi}$ defined from the $\overline{x}$-axis in the $\overline{x}$–$\overline{y}$–plane, for this two-dimensional problem independent of $\overline{y}$ we must have $I(\overline{\theta}, \overline{\psi}) = I(\overline{\theta}, -\overline{\psi})$ and, therefore, all $\overline{I}_n^m$ with negative m vanish. Thus, from equation (16.70), eliminating all terms with negative m and $\overline{y}$-gradients, we obtain

$$\begin{aligned}
\overline{Y}_1^0 :&\quad p_{01}^0 \overline{I}_0^0 + p_{21}^0 \overline{I}_2^0 + \frac{\partial}{\partial \tau_{\overline{x}}}\left[v_{11}^0 \overline{I}_2^1\right] - \frac{\partial}{\partial \tau_{\overline{z}}}\left[w_{01}^0 \overline{I}_0^0 + w_{11}^0 \overline{I}_2^0\right] = I_{bw} p_{01}^0, \\
\overline{Y}_1^1 :&\quad p_{21}^1 \overline{I}_2^1 - \frac{\partial}{\partial \tau_{\overline{x}}}\left[2u_{01}^1 \overline{I}_0^0 + 2u_{11}^1 \overline{I}_2^0 - v_{11}^1 \overline{I}_2^2\right] - \frac{\partial}{\partial \tau_{\overline{z}}}\left[w_{11}^1 \overline{I}_2^1\right] = 0, \\
\overline{Y}_3^0 :&\quad p_{03}^0 \overline{I}_0^0 + p_{23}^0 \overline{I}_2^0 + \frac{\partial}{\partial \tau_{\overline{x}}}\left[v_{12}^0 \overline{I}_2^1\right] - \frac{\partial}{\partial \tau_{\overline{z}}}\left[w_{02}^0 \overline{I}_0^0 + w_{12}^0 \overline{I}_2^0\right] = I_{bw} p_{03}^0, \\
\overline{Y}_3^2 :&\quad p_{23}^2 \overline{I}_2^2 - \frac{\partial}{\partial \tau_{\overline{x}}}\left[u_{12}^2 \overline{I}_2^1\right] - \frac{\partial}{\partial \tau_{\overline{z}}}\left[w_{12}^2 \overline{I}_2^2\right] = 0.
\end{aligned}$$

The equations for $\overline{Y}_1^{-1}$ and $\overline{Y}_3^{-2}$ contain only $\overline{I}_n^m$ with negative m and, thus, vanish identically, leaving us with the proper four boundary conditions for the four unknown $\overline{I}_n^m$. The coefficients p_{nj}^m, u_{li}^m, v_{li}^m, and w_{li}^m

are found from Table 16.2 [or, more easily from program `pnbcs.f90` in Appendix F] as

$$
\begin{aligned}
&p_{01}^0 = \frac{1}{2},\; p_{21}^0 = \frac{1}{8},\; p_{21}^1 = \frac{3}{4},\; p_{03}^0 = -\frac{1}{8},\; p_{23}^0 = \frac{1}{8},\; p_{23}^2 = \frac{15}{2};\\
&u_{01}^1 = \frac{-p_{11}^1}{2\cdot 1} = -\frac{1}{3},\; u_{11}^1 = \frac{p_{11}^1 - p_{31}^1}{2\cdot 5} = \frac{1}{10}\left(\frac{2}{3} - 0\right) = \frac{1}{15},\; u_{12}^2 = \frac{p_{13}^2 - p_{33}^2}{2\cdot 5} = \frac{1}{10}\left(0 - \frac{120}{7}\right) = -\frac{12}{7};\\
&v_{11}^0 = \frac{2\cdot 3p_{11}^0 - 2\cdot 3p_{31}^0}{2\cdot 5} = \frac{3}{5}\left(\frac{1}{3} - 0\right) = \frac{1}{5},\; v_{11}^1 = \frac{3\cdot 4p_{11}^1 - 1\cdot 2p_{31}^1}{2\cdot 5} = \frac{1}{10}\left(12\times\frac{2}{3} - 0\right) = \frac{4}{5},\\
&v_{12}^0 = \frac{2\cdot 3p_{13}^0 - 2\cdot 3p_{33}^0}{2\cdot 5} = \frac{3}{5}\left(0 - \frac{1}{7}\right) = -\frac{3}{35};\\
&w_{01}^0 = \frac{1\cdot p_{11}^0}{1} = \frac{1}{3},\; w_{11}^0 = \frac{2p_{11}^0 + 3p_{31}^0}{5} = \frac{1}{5}\left(\frac{2}{3} - 0\right) = \frac{2}{15},\; w_{11}^1 = \frac{3p_{11}^1 + 2p_{31}^1}{5} = \frac{1}{5}\left(3\times\frac{2}{3} + 0\right) = \frac{2}{5},\\
&w_{02}^0 = \frac{1\cdot p_{13}^0}{1} = 0,\; w_{12}^0 = \frac{2p_{13}^0 + 3p_{33}^0}{5} = \frac{1}{5}\left(0 + \frac{3}{7}\right) = \frac{3}{35},\; w_{12}^2 = \frac{4p_{13}^2 + 1\cdot p_{33}^2}{5} = \frac{1}{5}\left(0 + \frac{120}{7}\right) = \frac{24}{7}.
\end{aligned}
$$

Therefore, after normalization with the leading term,

$$\overline{Y}_1^0: \quad \overline{I}_0^0 + \frac{1}{4}\overline{I}_2^0 + \frac{2}{5}\frac{\partial \overline{I}_2^1}{\partial \tau_{\overline{x}}} - \frac{2}{3}\frac{\partial \overline{I}_0^0}{\partial \tau_{\overline{z}}} - \frac{4}{15}\frac{\partial \overline{I}_2^0}{\partial \tau_{\overline{z}}} = I_{bw}, \tag{16.76a}$$

$$\overline{Y}_1^1: \quad \overline{I}_2^1 + \frac{\partial}{\partial \tau_{\overline{x}}}\left[\frac{8}{9}\overline{I}_0^0 - \frac{8}{45}\overline{I}_2^0 + \frac{16}{15}\overline{I}_2^2\right] - \frac{8}{15}\frac{\partial \overline{I}_2^1}{\partial \tau_{\overline{z}}} = 0, \tag{16.76b}$$

$$\overline{Y}_3^0: \quad \overline{I}_0^0 - \overline{I}_2^0 + \frac{24}{35}\frac{\partial \overline{I}_2^1}{\partial \tau_{\overline{x}}} + \frac{24}{35}\frac{\partial \overline{I}_2^0}{\partial \tau_{\overline{z}}} = I_{bw}, \tag{16.76c}$$

$$\overline{Y}_3^2: \quad \overline{I}_2^2 + \frac{8}{35}\frac{\partial \overline{I}_2^1}{\partial \tau_{\overline{x}}} - \frac{16}{35}\frac{\partial \overline{I}_2^2}{\partial \tau_{\overline{z}}} = 0. \tag{16.76d}$$

Next, the local $\overline{I}_n^m$ must be converted to global I_n^m with equation (16.68). For $n = 0$ this simply gives $\overline{I}_0^0 = I_0^0$, i.e., I_0^0 is nondirectional and does not vary with rotation, and we will drop the unnecessary superscript from I_0. Remembering that, in global coordinates, I_n^m with odd m vanish (as opposed to negative m in local coordinates), for $n = 2$ this leads to

$$
\begin{aligned}
\overline{I}_2^0 &= \bar{\Delta}_{0,-2}^2 I_2^{-2} + \bar{\Delta}_{0,0}^2 I_2^0 + \bar{\Delta}_{0,2}^2 I_2^2,\\
\overline{I}_2^1 &= \bar{\Delta}_{1,-2}^2 I_2^{-2} + \bar{\Delta}_{1,0}^2 I_2^0 + \bar{\Delta}_{1,2}^2 I_2^2,\\
\overline{I}_2^2 &= \bar{\Delta}_{2,-2}^2 I_2^{-2} + \bar{\Delta}_{2,0}^2 I_2^0 + \bar{\Delta}_{2,2}^2 I_2^2.
\end{aligned}
$$

The necessary $\bar{\Delta}_{m,m'}^2(-\gamma = -\frac{\pi}{2}, -\beta = -\frac{3\pi}{2}, -\alpha = \frac{\pi}{2} - \delta)$ are determined via backward rotation from equation (16.65) with

$$\Psi_m\left(-\frac{\pi}{2}\right) = \begin{cases} -1, & m = 2\\ 0, & 1\\ 1, & 0\\ -1, & -1\\ 0, & -2 \end{cases}, \quad \Psi_{m'}\left(\frac{\pi}{2} - \delta\right) = \begin{cases} -\cos 2\delta, & m' = 2\\ \sin\delta, & 1\\ 1, & 0\\ \cos\delta, & -1\\ \sin 2\delta, & -2 \end{cases},$$

and $\cos(\frac{\beta}{2}) = \sin(\frac{\beta}{2}) = \cos(-\frac{3\pi}{4}) = -\frac{1}{\sqrt{2}}$. The $d_{mm'}^2$ follow from equation (16.67) after some painful algebra (or, more easily, by manipulating program `Delta.f90` in Appendix F). Finally,

$$
\begin{aligned}
\overline{I}_2^0 &= -3\sin 2\delta\, I_2^{-2} - \frac{1}{2}I_2^0 - 3\cos 2\delta\, I_2^2,\\
\overline{I}_2^1 &= -2\cos 2\delta\, I_2^{-2} + 2\sin 2\delta\, I_2^2,\\
\overline{I}_2^2 &= \frac{1}{2}\sin 2\delta\, I_2^{-2} - \frac{1}{4}I_2^0 + \frac{1}{2}\cos 2\delta\, I_2^2.
\end{aligned}
$$

Sticking this into equation (16.76) delivers the desired local boundary conditions as

$$\begin{aligned}
\overline{Y}_1^0 : \quad & I_0 - \frac{3}{4}\sin 2\delta\, I_2^{-2} - \frac{1}{8} I_2^0 - \frac{3}{4}\cos 2\delta\, I_2^2 - \frac{4}{5}\frac{\partial}{\partial \tau_{\overline{x}}}\left[\cos 2\delta\, I_2^{-2} - \sin 2\delta\, I_2^2\right] \\
& - \frac{2}{15}\frac{\partial}{\partial \tau_{\overline{z}}}\left[5I_0 - 6\sin 2\delta\, I_2^{-2} - I_2^0 - 6\cos 2\delta\, I_2^2\right] = I_w, \\
\overline{Y}_1^1 : \quad & -2\cos 2\delta\, I_2^{-2} + 2\sin 2\delta\, I_2^2 + \frac{8}{45}\frac{\partial}{\partial \tau_{\overline{x}}}\left[5I_0 - I_2 + 6\sin 2\delta\, I_2^{-2} + 6\cos 2\delta\, I_2^2\right] \\
& + \frac{48}{45}\frac{\partial}{\partial \tau_{\overline{z}}}\left[\cos 2\delta\, I_2^{-2} - \sin 2\delta\, I_2^2\right] = 0, \\
\overline{Y}_3^0 : \quad & I_0 + 3\sin 2\delta\, I_2^{-2} + \frac{1}{2} I_2^0 + 3\cos 2\delta\, I_2^2 - \frac{48}{35}\frac{\partial}{\partial \tau_{\overline{x}}}\left[\cos 2\delta\, I_2^{-2} - \sin 2\delta\, I_2^2\right] \\
& - \frac{24}{35}\frac{\partial}{\partial \tau_{\overline{z}}}\left[3\sin 2\delta\, I_2^{-2} + \frac{1}{2} I_2^0 + 3\cos 2\delta\, I_2^2\right] = I_w, \\
\overline{Y}_3^2 : \quad & \frac{1}{2}\sin 2\delta\, I_2^{-2} - \frac{1}{4} I_2^0 + \frac{1}{2}\cos 2\delta\, I_2^2 - \frac{16}{35}\frac{\partial}{\partial \tau_{\overline{x}}}\left[\cos 2\delta\, I_2^{-2} - \sin 2\delta\, I_2^2\right] \\
& - \frac{4}{35}\frac{\partial}{\partial \tau_{\overline{z}}}\left[2\sin 2\delta\, I_2^{-2} - I_2^0 + 2\cos 2\delta\, I_2^2\right] = 0.
\end{aligned}$$

Once all I_n^m for even n have been determined, the remaining I_n^m (odd n) may be determined from relations given in Modest and Yang [13]. Normally, only incident radiation $G = 4\pi I_0$ and radiative flux are of interest, the latter being related to the I_1^m: comparing equations (16.24), (16.25), and (16.31) and noting that higher-order terms drop out because of the orthogonality of spherical harmonics [14], leads to

$$\mathbf{q}(\mathbf{r}) = \int_{4\pi} I(\mathbf{r}, \hat{\mathbf{s}})\, \hat{\mathbf{s}}\, d\Omega = \frac{4\pi}{3}\begin{pmatrix} -I_1^1 \\ -I_1^{-1} \\ I_1^0 \end{pmatrix}, \tag{16.77}$$

where the I_1^m are given by [13]

$$I_1^0 = -\frac{\partial I_0}{\partial \tau_z} - \frac{2}{5}\frac{\partial I_2^0}{\partial \tau_z} + \frac{3}{5}\frac{\partial I_2^1}{\partial \tau_x} + \frac{3}{5}\frac{\partial I_2^{-1}}{\partial \tau_y}, \tag{16.78a}$$

$$I_1^1 = +\frac{\partial I_0}{\partial \tau_x} - \frac{1}{5}\frac{\partial I_2^0}{\partial \tau_x} - \frac{3}{5}\frac{\partial I_2^1}{\partial \tau_z} + \frac{6}{5}\frac{\partial I_2^2}{\partial \tau_x} + \frac{6}{5}\frac{\partial I_2^{-2}}{\partial \tau_y}, \tag{16.78b}$$

$$I_1^{-1} = +\frac{\partial I_0}{\partial \tau_y} - \frac{1}{5}\frac{\partial I_2^0}{\partial \tau_y} - \frac{3}{5}\frac{\partial I_2^{-1}}{\partial \tau_z} - \frac{6}{5}\frac{\partial I_2^2}{\partial \tau_y} + \frac{6}{5}\frac{\partial I_2^{-2}}{\partial \tau_x}. \tag{16.78c}$$

Since equation (16.1) is valid for any coordinate system orientation, equations (16.77) and (16.78) are valid for both the global coordinate system (x-y-z, I_n^m) as well as a local coordinate system at a boundary ($\overline{x}$-$\overline{y}$-$\overline{z}$, $\overline{I}_n^m$).

Finally, for nonblack surfaces the boundary radiosity $J_w = \pi I_w$ must be related to the wall's emissive power and/or net radiative flux. From equations (16.1) and (16.77) we have

$$q_n = \frac{\epsilon\pi}{1-\epsilon}\left[I_{bw} - I_w\right] = \frac{4\pi}{3}\overline{I}_1^0, \tag{16.79}$$

where ϵ is the surface's emittance, and with $\overline{I}_1^0$ transformed to global I_1^m through equation (16.68). If the temperature of the surface, T_w, is specified, I_w is determined from

$$I_w = I_{bw} - \frac{4}{3}\left(\frac{1}{\epsilon} - 1\right)\overline{I}_1^0. \tag{16.80}$$

For three-dimensional geometries, it is obvious that anything but low-order approximations quickly become extremely cumbersome to deal with. Already the P_3-approximation may result in as many as six simultaneous partial differential equations (depending on the symmetry), and it includes cross-derivatives, which do not ordinarily occur in engineering problems (and which complicate numerical solutions). In addition, complicated boundary conditions need to be developed from equation (16.73). As a result of this complexity, very few multidimensional problems have been solved by the P_3-approximation, and apparently none by higher orders. First results using the new elliptic formulation of equations (16.54) and (16.73) have been reported by Modest and coworkers [13, 18, 48]. We shall limit ourselves here to a simple example for a one-dimensional plane-parallel slab.

Example 16.7. Consider an isothermal medium at temperature T, confined between two large, parallel black plates that are isothermal at the (same) temperature T_w. The medium is gray and absorbs and emits, but does not scatter. Determine an expression for the heat transfer rates within the medium using the P_3-approximation. Employ the results from the previous three examples.

Solution

For such a one-dimensional problem it is, generally, advantageous to choose τ_z as the (nondimensional) space coordinate between the plates, as was done in Example 16.2, since this will make all I_n^m vanish with $m \neq 0$. However, for demonstrative purposes, and to utilize results from the previous three examples, we will choose the global coordinate system of Fig. 16-6, i.e., the problem becomes one-dimensional in the y-direction, with the bottom surface corresponding to $\delta = 0$, and the top to $\delta = \pi$. Since now we have no x-dependence we must have $I(\theta, \psi) = I(\theta, \pi - \psi)$, which implies that we will not have any odd positive or even negative m terms in equation (16.56*a*). Together with $n + m =$ even (no z-dependence) that reduces the set of equations developed in Example 16.4 to

$$
\begin{aligned}
Y_0^0: &\quad \frac{d^2}{d\tau_y^2}\left(\frac{2}{5}I_2^2 + \frac{1}{15}I_2^0 - \frac{1}{3}I_0\right) + I_0 = I_b,\\
Y_2^0: &\quad \frac{d^2}{d\tau_y^2}\left(\frac{4}{7}I_2^2 + \frac{5}{21}I_2^0 - \frac{1}{3}I_0\right) - I_2^0 = 0,\\
Y_2^2: &\quad \frac{d^2}{d\tau_y^2}\left(\frac{3}{7}I_2^2 + \frac{1}{21}I_2^0 - \frac{1}{6}I_0\right) - I_2^2 = 0,
\end{aligned}
$$

and all terms vanish for the Y_2^{-2}-equation, i.e., we now have three equations in three unknowns (since $I_2^{-2} = 0$).

To exploit the symmetry of the problem, we choose the origin for τ_y to be at the midpoint between the two plates. Then the first derivatives of all three unknowns will be zero at the midpoint:

$$\tau_y = 0: \quad \frac{dI_0}{d\tau_y} = \frac{dI_2^0}{d\tau_y} = \frac{dI_2^2}{d\tau_y} = 0.$$

The necessary second set of boundary conditions follows from Example 16.6 with $\delta = 0$ at $\tau_y = -\tau_L/2$ (and τ_L is the total optical thickness of the medium) as

$$
\begin{aligned}
\overline{Y}_1^0: &\quad I_0 - \frac{1}{8}I_2^0 - \frac{3}{4}I_2^2 - \frac{2}{15}\frac{d}{d\tau_y}\left[5I_0 - I_2^0 - 6I_2^2\right] = I_{bw},\\
\overline{Y}_3^0: &\quad I_0 + \frac{1}{2}I_2^0 + 3I_2^2 - \frac{12}{35}\frac{d}{d\tau_y}\left[I_2^0 + 6I_2^2\right] = I_{bw},\\
\overline{Y}_3^2: &\quad -\frac{1}{4}I_2^0 + \frac{1}{2}I_2^2 + \frac{4}{35}\frac{d}{d\tau_y}\left[I_2^0 - 2I_2^2\right] = 0,
\end{aligned}
$$

with all terms in the $\overline{Y}_1^1$ boundary condition vanishing. While the given set of three simultaneous ordinary differential equations in I_0, I_2^0, and I_2^2, together with their boundary conditions, can be solved as they are, we do know from Section 16.3 that, for a one-dimensional problem, there should be only a single I_n^m for every n (i.e., I_n^0). Inspecting the governing equations and boundary conditions, we find that I_2^0 and I_2^2 always occur in one of two combinations, viz.

$$I_2 = -\frac{1}{2}\left(I_2^0 + 6I_2^2\right),$$
$$K_2 = I_2^0 - 2I_2^2,$$

where the factor $-\frac{1}{2}$ was included for convenience (i.e., I_2 just so happens to be I_2^0 for the case that the z-axis points from plate to plate). Then

$$\begin{aligned}
Y_0^0: &\quad -\frac{2}{15}I_2'' - \frac{1}{3}I_0'' + I_0 = I_b,\\
Y_2^0 + 6Y_2^2: &\quad -\frac{11}{21}I_2'' - \frac{2}{3}I_0'' + I_2 = 0,\\
Y_2^0 - 2Y_2^2: &\quad \frac{1}{7}K_2'' - K_2 = 0,
\end{aligned}$$

where the primes have been introduced as shorthand for $d/d\tau_y$. The boundary conditions at $\tau_y = -\tau_L/2$ follow as

$$\begin{aligned}
\overline{Y}_1^0: &\quad I_0 + \frac{1}{4}I_2 - \frac{2}{3}I_0' - \frac{4}{15}I_2' = I_{bw},\\
\overline{Y}_3^0: &\quad I_0 - I_2 + \frac{24}{35}I_2' = I_{bw},\\
\overline{Y}_3^2: &\quad \frac{1}{2}K_2 + \frac{4}{35}K_2' = 0.
\end{aligned}$$

It follows that $K_2 \equiv 0$, since both its governing equation and its boundary conditions are homogeneous. I_2 can be eliminated from the remaining equations: first we eliminate I_2'' from the first two equations, leading to

$$-\frac{9}{55}I_0'' + I_0 - \frac{14}{55}I_2 = I_b,$$

or

$$I_2 = -\frac{9}{14}I_0'' + \frac{55}{14}\left(I_0 - I_b\right).$$

Differentiating twice and eliminating I_2'' from the Y_0^0 equation, we obtain

$$\frac{3}{35}I_0^{(iv)} - \frac{6}{7}I_0'' + I_0 = I_b.$$

The general solution to the above equation (keeping in mind that I_b = const) is

$$I_0(\tau_y) = I_b + (I_{bw} - I_b)[C_1\cosh\lambda_1\tau_y + C_2\cosh\lambda_2\tau_y + C_3\sinh\lambda_1\tau_y + C_4\sinh\lambda_2\tau_y],$$

where the constant factor $(I_{bw} - I_b)$ was included to make the C_i dimensionless. The λ_1 and λ_2 are the positive roots of the equation

$$\frac{3}{35}\lambda^4 - \frac{6}{7}\lambda^2 + 1 = 0,$$

or $\lambda_1 = 1.1613$ and $\lambda_2 = 2.9413$. With $\tau_y = 0$ placed at the midpoint between the two plates $I_0'(0) = I_0'''(0) = 0$ and $C_3 = C_4 = 0$. The two needed boundary conditions at one of the plates, say at $\tau = -\tau_L/2$, are found by again eliminating I_2, or

$$\begin{aligned}
\overline{Y}_1^0: &\quad I_0 + \frac{1}{4}\left[-\frac{9}{14}I_0'' + \frac{55}{14}\left(I_0 - I_b\right)\right] - \frac{2}{3}I_0' - \frac{4}{15}\left[-\frac{9}{14}I_0''' + \frac{55}{14}I_0'\right] = I_{bw},\\
\overline{Y}_3^0: &\quad I_0 - \left[-\frac{9}{14}I_0'' + \frac{55}{14}\left(I_0 - I_b\right)\right] + \frac{24}{35}\left[-\frac{9}{14}I_0''' + \frac{55}{14}I_0'\right] = I_{bw},
\end{aligned}$$

leading to

$$I_{bw}-I_b = \frac{111}{56}(I_0-I_b)-\frac{12}{7}I_0'-\frac{9}{56}I_0''+\frac{6}{35}I_0''',$$

$$I_{bw}-I_b = -\frac{41}{14}(I_0-I_b)+\frac{132}{49}I_0'+\frac{9}{14}I_0''-\frac{108}{245}I_0'''.$$

Now, substituting the solution for I_0 into these boundary conditions leads to

$$1 = a_1C_1+a_2C_2 = b_1C_1+b_2C_2,$$

where

$$a_i = \left(\frac{111}{56}-\frac{9}{56}\lambda_i^2\right)\cosh\lambda_i\frac{\tau_L}{2}+\left(\frac{12}{7}\lambda_i-\frac{6}{35}\lambda_i^3\right)\sinh\lambda_i\frac{\tau_L}{2}, \quad i=1,2,$$

$$b_i = -\left(\frac{41}{74}-\frac{9}{14}\lambda_i^2\right)\cosh\lambda_i\frac{\tau_L}{2}-\left(\frac{132}{49}\lambda_i-\frac{108}{245}\lambda_i^3\right)\sinh\lambda_i\frac{\tau_L}{2}, \quad i=1,2.$$

Finally, we get

$$C_1=\frac{b_2-a_2}{a_1b_2-a_2b_1}, \qquad C_2=\frac{a_1-b_1}{a_1b_2-a_2b_1}.$$

The heat flux through the medium is determined from equations (16.77) and (16.78) as

$$q(\tau_y) = -\frac{4\pi}{3}I_1^{-1} = -\frac{4\pi}{3}\left(\frac{\partial I_0}{\partial\tau_y}-\frac{1}{5}\frac{\partial I_2^0}{\partial\tau_y}-\frac{6}{5}\frac{\partial I_2^2}{\partial\tau_y}\right) = -\frac{4\pi}{3}\left(\frac{\partial I_0}{\partial\tau_y}+\frac{2}{5}\frac{\partial I_2}{\partial\tau_y}\right).$$

Substituting for I_2 we obtain

$$q(\tau_y) = -\frac{4\pi}{3}\left(I_0'-\frac{9}{35}I_0'''+\frac{11}{7}I_0'\right),$$

and the heat flux may be expressed in nondimensional form as

$$\Psi = \frac{q(\tau_y)}{n^2\sigma(T_w^4-T^4)} = -\frac{12}{35}\frac{10I_0'-I_0'''}{I_{bw}-I_b} = -\frac{12}{35}\sum_{i=1}^{2}(10\lambda_i-\lambda_i^3)C_i\sinh\lambda_i\tau_y,$$

where, for simplicity, it was assumed that the medium is gray, or $I_b=n^2\sigma T^4/\pi$.

The nondimensional heat flux at the top surface ($\tau_y=\tau_L/2$) is shown in Fig. 16-8, as a function of optical depth of the slab. The results are compared with those of the P_1- or *differential approximation* (Example 16.2), and with the exact result,

$$\Psi = 1-2E_3(\tau_L),$$

which is readily found from equation (14.35). For this particular example the P_1-approximation is very accurate (maximum error ~15%) and, as to be expected, the P_3-approximation performs even better (maximum error ~7%).

It should be clear from the above example that P_3- and higher-order P_N-approximations quickly become very tedious, even for simple geometries. However, P_3 results can be substantially more accurate than P_1 results, particularly in optically thin media and/or geometries with large aspect ratios. Another example, shown in Fig. 16-5, depicts nondimensional heat flux through a gray, nonscattering medium at radiative equilibrium, confined between infinitely long, concentric, black and isothermal cylinders, in which the P_3-solution of Bayazitoğlu and Higenyi [24] is compared with the P_1-solution (Example 16.3). Observe that the P_3-approximation introduces roughly half the error of the P_1-method, which appears to be approximately true for all problems. One outstanding advantage of the P_3-method is that, once the problem has been formulated (setting up the governing equations suitable for a numerical solution), the increase in computer time required (compared with the P_1-method) is relatively minor. In addition, P_3-calculations are also usually very grid-compatible with conduction/convection calculations, if one must account for combined modes of heat transfer. Three additional two-dimensional examples will be presented in the final section of this chapter, comparing results from different orders and different schemes of the spherical harmonics method.

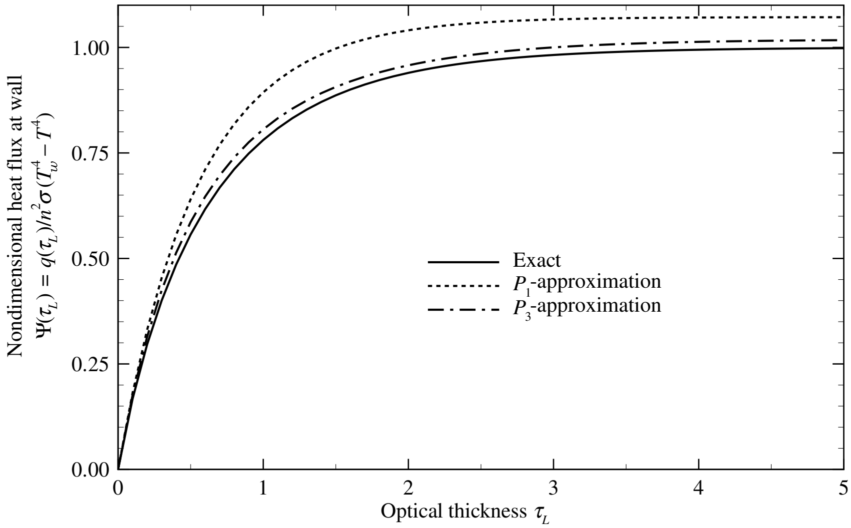

FIGURE 16-8
Nondimensional wall heat fluxes for an isothermal slab; comparison of P_1- and P_3-approximations with the exact solution.

16.7 SIMPLIFIED P_N-APPROXIMATION

As noted in the previous section, higher-order P_N-formulations for anything but one-dimensional slabs become extremely cumbersome mathematically, and they also introduce cross-derivatives, which make a numerical solution considerable more involved. Facing these mathematical difficulties Gelbard [5] introduced the *Simplified P_N-Approximation* some 50 years ago, as an intuitive three-dimensional extension to the one-dimensional slab P_N-formulation, equation (16.14), and its Marshak boundary conditions, equations (16.21). Gelbard formulated his set of simplified-P_N or SP_N equations, such that they reduced to the standard P_N-approximation for a one-dimensional slab and some other narrow circumstances, but the method lacked any theoretical foundation, which impeded its acceptance. Theoretical justifications were found many years later by Larsen *et al.* [54] (showing SP_N to be an asymptotic correction to the diffusion approximation of Section 15.2) and by Pomraning [55] (showing the SP_N to be asymptotically related to the P_N-equations for the slab geometry). A fine review of the SP_N-method has recently been given by McClarren [56].

While the developments of Larsen and Pomraning provide theoretical credentials to the method, they are rather tedious, and we will here only provide the intuitive development of Gelbard, further developed for radiative heat transfer applications by Modest [57]. Depending on whether k is odd or even, Gelbard made the following substitutions in equations (16.14) and (16.21):

$$k \text{ odd}: \qquad I_k(\tau) \to \mathbf{I}_k(\tau_x, \tau_y, \tau_z), \qquad I'_k = \frac{dI_k}{d\tau} \to \nabla_\tau \cdot \mathbf{I}_k, \tag{16.81a}$$

$$k \text{ even}: \qquad I_k(\tau) \to I_k(\tau_x, \tau_y, \tau_z), \qquad I'_k = \frac{dI_k}{d\tau} \to \nabla_\tau I_k, \tag{16.81b}$$

i.e., for every odd k the I_k becomes a vector and differentiation is replaced by the divergence operator, while even I_k remain scalars and their differentiation is replaced by the gradient operator. Substituting equations (16.81) into equation (16.14) leads to

$$k = 0, 2, \ldots, N-1 \quad (\text{even}): \qquad \frac{k+1}{2k+3}\nabla_\tau \cdot \mathbf{I}_{k+1} + \frac{k}{2k-1}\nabla_\tau \cdot \mathbf{I}_{k-1} + \alpha_k I_k = \alpha_k I_b \delta_{0k}, \tag{16.82a}$$

$$k = 1, 3, \ldots, N \quad (\text{odd}): \qquad \frac{k+1}{2k+3}\nabla_\tau I_{k+1} + \frac{k}{2k-1}\nabla_\tau I_{k-1} + \alpha_k \mathbf{I}_k = 0, \tag{16.82b}$$

where

$$\alpha_k = 1 - \frac{\omega A_k}{2k+1}. \tag{16.82c}$$

Solving equation (16.82*b*) for $\mathbf{I}_k$ and substituting the result into (16.82*a*) produces a set of simultaneous elliptic partial differential equations in the unknown scalars I_k (k even):

$$\begin{aligned}
&k = 0, 2, \ldots, N-1 \quad \text{(even)}: \\
&\quad \frac{(k+1)(k+2)}{(2k+3)(2k+5)} \boldsymbol{\nabla}_\tau \cdot \left(\frac{1}{\alpha_{k+1}} \boldsymbol{\nabla}_\tau I_{k+2} \right) + \frac{(k+1)^2}{(2k+3)(2k+1)} \boldsymbol{\nabla}_\tau \cdot \left(\frac{1}{\alpha_{k+1}} \boldsymbol{\nabla}_\tau I_k \right) \\
&\quad + \frac{k^2}{(2k-1)(2k+1)} \boldsymbol{\nabla}_\tau \cdot \left(\frac{1}{\alpha_{k-1}} \boldsymbol{\nabla}_\tau I_k \right) + \frac{k(k-1)}{(2k-1)(2k-3)} \boldsymbol{\nabla}_\tau \cdot \left(\frac{1}{\alpha_{k-1}} \boldsymbol{\nabla}_\tau I_{k-2} \right) = \alpha_k (I_k - I_b \delta_{0k}).
\end{aligned} \tag{16.83}$$

Similarly, sticking equations (16.81) into the P_N boundary conditions, equations (16.21), gives us a consistent set of conditions for the SP_N-equations:

$$\sum_{k\text{ even}}^{N-1} I_k \int_0^1 P_k(\mu) P_{2i-1}(\mu)\, d\mu + \sum_{k\text{ odd}}^{N} \hat{\mathbf{n}} \cdot \mathbf{I}_k \int_0^1 P_k(\mu) P_{2i-1}(\mu)\, d\mu = \frac{J_w}{\pi} \int_0^1 P_{2i-1}(\mu)\, d\mu, \qquad i = 1, 2, \ldots, \tfrac{1}{2}(N+1), \tag{16.84}$$

or, with the definition of the Legendre polynomial half-moments $p^m_{n,j}$ given by equation (16.71),

$$\sum_{k\text{ even}}^{N-1} p^0_{k,2i-1} I_k + \sum_{k\text{ odd}}^{N} p^0_{k,2i-1} \hat{\mathbf{n}} \cdot \mathbf{I}_k = \frac{p^0_{0,2i-1}}{\pi} J_w, \qquad i = 1, 2, \ldots, \tfrac{1}{2}(N+1). \tag{16.85}$$

Again, eliminating the odd $\mathbf{I}_k$ with equation (16.82*b*), this set of boundary conditions reduces to

$$\sum_{k\text{ even}}^{N-1} p^0_{k,2i-1} I_k - \sum_{k\text{ odd}}^{N} \frac{p^0_{k,2i-1}}{\alpha_k} \left[\frac{k}{2k-1} \hat{\mathbf{n}} \cdot \boldsymbol{\nabla}_\tau I_{k-1} + \frac{k+1}{2k+3} \hat{\mathbf{n}} \cdot \boldsymbol{\nabla}_\tau I_{k+1} \right] = \frac{p^0_{0,2i-1}}{\pi} J_w \qquad i = 1, 2, \ldots, \tfrac{1}{2}(N+1). \tag{16.86}$$

No direct formula for intensity is derived, but one may assume a series of the form

$$I(\mathbf{r}, \hat{\mathbf{s}}) = I_0(\mathbf{r}) + \mathbf{I}_1(\mathbf{r}) \cdot \hat{\mathbf{s}} + I_2(\mathbf{r}) P^0_2(\hat{\mathbf{s}}) + \ldots, \tag{16.87}$$

which is no longer a complete series of orthogonal functions and, therefore, is not guaranteed to approach the exact answer in the limit. However, assuming this to be an orthogonal set, we can obtain incident radiation G and radiative flux $\mathbf{q}$ from their definitions as

$$G(\mathbf{r}) = \int_{4\pi} I(\mathbf{r}, \hat{\mathbf{s}})\, d\Omega = 4\pi I_0(\mathbf{r}), \tag{16.88}$$

$$\mathbf{q}(\mathbf{r}) = \int_{4\pi} I(\mathbf{r}, \hat{\mathbf{s}})\, \hat{\mathbf{s}}\, d\Omega = \frac{4\pi}{3} \mathbf{I}_1(\mathbf{r}) = -\frac{4\pi}{3\alpha_1} \left[\boldsymbol{\nabla}_\tau I_0 + \frac{2}{5} \boldsymbol{\nabla}_\tau I_2 \right]. \tag{16.89}$$

While equations (16.83) and (16.86) form a self-consistent set of $(N+1)/2$ simultaneous elliptic partial differential equations and their boundary conditions, the problem can be further simplified by recognizing that the combination of variables

$$J_k = \frac{k+1}{2k+1} I_k + \frac{k+2}{2k+5} I_{k+2} \tag{16.90}$$

appears repeatedly in both the governing equations and boundary conditions. In addition, inspection of Table 16.2 shows that $p^0_{n,j} = 0$ if $n + j =$ even, with the exception of $n = j$. Thus we may rewrite equations (16.83) as

$$k = 0, 2, \ldots, N-1 \quad \text{(even)}:$$
$$\frac{k+1}{2k+3}\boldsymbol{\nabla}_\tau \cdot \left(\frac{1}{\alpha_{k+1}}\boldsymbol{\nabla}_\tau J_k\right) + \frac{k}{2k-1}\boldsymbol{\nabla}_\tau \cdot \left(\frac{1}{\alpha_{k-1}}\boldsymbol{\nabla}_\tau J_{k-2}\right) = \alpha_k(I_k - I_b\delta_{0k}), \tag{16.91}$$

and boundary conditions (16.86) as

$$\frac{p^0_{2i-1,2i-1}}{\alpha_{2i-1}}\hat{\mathbf{n}} \cdot \boldsymbol{\nabla}_\tau J_{2i-2} = \sum_{k=0}^{\frac{N-1}{2}} p^0_{2k,2i-1} I_{2k} - \frac{p^0_{0,2i-1}}{\pi} J_w, \qquad i = 1, 2, \ldots, \tfrac{1}{2}(N+1). \tag{16.92}$$

The I_k on the right-hand sides may be eliminated by inverting equation (16.90), starting with $k = N - 1$ (and noting that $I_{N+1} \equiv 0$). This results in individual partial differential equations for each J_k, in which J_l ($l \neq k$) occur only as source terms without derivatives. Once the J_k have been determined, incident radiation and radiative flux are obtained from equations (16.88) and (16.89) as

$$G(\mathbf{r}) = 4\pi\left[J_0(\mathbf{r}) - \frac{2}{3}J_2(\mathbf{r}) + \frac{24}{55}J_4(\mathbf{r}) - + \ldots\right], \tag{16.93}$$
$$\mathbf{q}(\mathbf{r}) = -\frac{4\pi}{3\alpha_1}\boldsymbol{\nabla}_\tau J_0(\mathbf{r}). \tag{16.94}$$

We will demonstrate this by looking in more detail at the SP_1- and SP_3-approximations (even orders, such as SP_2, have also been formulated [58], but—based on the development shown here—appear to be as inappropriate as for the standard P_N-method).

SP_1-Approximation

With $N = 1$ we obtain a single equation and a single boundary condition from equations (16.91) and (16.92), i.e.:
Governing equation:

$$k = 0: \qquad \frac{1}{3}\boldsymbol{\nabla}_\tau \cdot \left(\frac{1}{\alpha_1}\boldsymbol{\nabla}_\tau J_0\right) = \alpha_0(I_0 - I_b); \tag{16.95}$$

Boundary condition:

$$i = 1: \qquad \frac{p^0_{1,1}}{\alpha_1}\hat{\mathbf{n}} \cdot \boldsymbol{\nabla}_\tau J_0 = p^0_{0,1}(I_0 - J_w/\pi). \tag{16.96}$$

With $p^0_{0,1} = \frac{1}{2}$ and $p^0_{1,1} = \frac{1}{3}$ from Table 16.2, and $I_0 = J_0$ from equation (16.90), we obtain

$$\frac{1}{3}\boldsymbol{\nabla}_\tau \cdot \left(\frac{1}{\alpha_1}\boldsymbol{\nabla}_\tau J_0\right) = \alpha_0(J_0 - I_b), \tag{16.97}$$

with boundary condition

$$\frac{1}{3\alpha_1}\hat{\mathbf{n}} \cdot \boldsymbol{\nabla}_\tau J_0 = \frac{1}{2}(J_0 - J_w/\pi). \tag{16.98}$$

Not surprisingly, comparison with equations (16.38) and (16.49) and using $G = 4\pi I_0 = 4\pi J_0$ shows that the SP_1-approximation is identical to the P_1-method.

SP_3-Approximation

Setting $N = 3$ we get two simultaneous equations and two boundary conditions:
Governing equations:

$$k=0: \qquad \frac{1}{3}\boldsymbol{\nabla}_\tau \cdot \left(\frac{1}{\alpha_1}\boldsymbol{\nabla}_\tau J_0\right) = \alpha_0(I_0 - I_b) = \alpha_0\left(J_0 - \frac{2}{3}J_2 - I_b\right), \tag{16.99a}$$

$$k=2: \qquad \frac{3}{7}\boldsymbol{\nabla}_\tau \cdot \left(\frac{1}{\alpha_3}\boldsymbol{\nabla}_\tau J_2\right) + \frac{2}{3}\boldsymbol{\nabla}_\tau \cdot \left(\frac{1}{\alpha_1}\boldsymbol{\nabla}_\tau J_0\right) = \alpha_2 I_2 = \frac{5}{3}\alpha_2 J_2, \tag{16.99b}$$

or, subtracting $2\times$ equation (16.99*a*),

$$k=2: \qquad \frac{3}{7}\boldsymbol{\nabla}_\tau \cdot \left(\frac{1}{\alpha_3}\boldsymbol{\nabla}_\tau J_2\right) = \left(\frac{5}{3}\alpha_2 + \frac{4}{3}\alpha_0\right)J_2 - 2\alpha_0(J_0 - I_b). \tag{16.99c}$$

Boundary conditions:

$$i=1: \qquad \frac{p^0_{1,1}}{\alpha_1}\hat{\mathbf{n}}\cdot\boldsymbol{\nabla}_\tau J_0 = p^0_{0,1}(I_0 - J_w/\pi) + p^0_{2,1}I_2, \tag{16.100a}$$

$$i=2: \qquad \frac{p^0_{3,3}}{\alpha_3}\hat{\mathbf{n}}\cdot\boldsymbol{\nabla}_\tau J_2 = p^0_{0,3}(I_0 - J_w/\pi) + p^0_{2,3}I_2. \tag{16.100b}$$

With $p^0_{2,1} = p^0_{2,3} = \frac{1}{8}$, $p^0_{3,3} = \frac{1}{7}$, $p^0_{0,3} = -\frac{1}{8}$, and eliminating the I_k, the boundary conditions become

$$i=1: \qquad \frac{1}{3\alpha_1}\hat{\mathbf{n}}\cdot\boldsymbol{\nabla}_\tau J_0 = \tfrac{1}{2}(J_0 - \tfrac{2}{3}J_2 - J_w/\pi) + \tfrac{1}{8}\tfrac{5}{3}J_2 = \tfrac{1}{2}(J_0 - J_w/\pi) - \tfrac{1}{8}J_2, \tag{16.100c}$$

$$i=2: \qquad \frac{1}{7\alpha_3}\hat{\mathbf{n}}\cdot\boldsymbol{\nabla}_\tau J_2 = -\tfrac{1}{8}(J_0 - \tfrac{2}{3}J_2 - J_w/\pi) + \tfrac{1}{8}\tfrac{5}{3}J_2 = -\tfrac{1}{8}(J_0 - J_w/\pi) + \tfrac{7}{24}J_2. \tag{16.100d}$$

Unlike the regular P_3-approximation, SP_3 has only two, and nearly separated, elliptic partial differential equations: equations (16.99*a*) and (16.100*c*) for J_0 and equations (16.99*c*) and (16.100*d*) for J_2, the only connection being the other J_k appearing in source terms.

Example 16.8. Repeat Examples 16.4, 16.6, and 16.7 using the SP_3-approximation.

Solution
For a nonscattering medium without z-dependence equations (16.99) reduce to

$$\begin{aligned}
\frac{1}{3}(\mathscr{L}_{xx} + \mathscr{L}_{yy})J_0 - J_0 &= -\frac{2}{3}J_2 - I_b,\\
\frac{1}{7}(\mathscr{L}_{xx} + \mathscr{L}_{yy})J_2 - J_2 &= -\frac{2}{3}(J_0 - I_b),
\end{aligned}$$

where we have used the operators defined in equation (16.53) for better comparison with the equivalent P_3 set of Example 16.4.

The boundary conditions for a general location simplify to

$$\begin{aligned}
\frac{1}{3}\frac{\partial J_0}{\partial \tau_{\bar{z}}} &= \frac{1}{2}(J_0 - I_b) - \frac{1}{8}J_2,\\
\frac{1}{7}\frac{\partial J_2}{\partial \tau_{\bar{z}}} &= -\frac{1}{8}(J_0 - I_b) + \frac{7}{24}J_2.
\end{aligned}$$

Finally, for the one-dimensional case with only y-dependence, and again taking advantage of the symmetry by placing $\tau_y = 0$ at the midplane, the equations and boundary conditions further reduce to

$$\begin{aligned}
\frac{1}{3}J_0'' - J_0 &= -\frac{2}{3}J_2 - I_b,\\
\frac{1}{7}J_2'' - J_2 &= -\frac{2}{3}(J_0 - I_b),
\end{aligned}$$

$$\tau_y = 0: \qquad J_0' = J_2' = 0,$$
$$\tau_y = -\tau_L/2: \qquad \frac{1}{3}J_0' = \frac{1}{2}(J_0 - I_{bw}) - \frac{1}{8}J_2,$$
$$\frac{1}{7}J_2' = -\frac{1}{8}(J_0 - I_{bw}) + \frac{7}{24}J_2.$$

The set of two simultaneous equations is readily reduced to one, by solving the first for J_2:

$$J_2 = \frac{3}{2}(J_0 - I_b) - \frac{1}{2}J_0'',$$

then substituting for J_2 and J_2'' in the second, or

$$\frac{1}{7}\left[\frac{3}{2}J_0'' - \frac{1}{2}J_0^{(iv)}\right] - \left[\frac{3}{2}(J_0 - I_b) - \frac{1}{2}J_0''\right] = -\frac{2}{3}(J_0 - I_b),$$

or

$$\frac{3}{35}J_0^{(iv)} - \frac{6}{7}J_0'' + J_0 = I_b.$$

Similarly, we eliminate J_2 from the boundary conditions:

$$\tau_y = 0: \qquad J_0' = J_0''' = 0,$$
$$\tau_y = -\tau_L/2: \qquad \frac{1}{3}J_0' = \frac{1}{2}(J_0 - I_{bw}) - \frac{1}{8}\left[\frac{3}{2}(J_0 - I_b) - \frac{1}{2}J_0''\right],$$
$$\frac{1}{7}\left[\frac{3}{2}J_0' - \frac{1}{2}J_0'''\right] = -\frac{1}{8}(J_0 - I_{bw}) + \frac{7}{24}\left[\frac{3}{2}(J_0 - I_b) - \frac{1}{2}J_0''\right],$$

leading to

$$\tau_y = -\tau_L/2: \qquad I_{bw} - I_b = \frac{5}{8}(J_0 - I_b) - \frac{2}{3}J_0' + \frac{1}{8}J_0''$$
$$I_{bw} - I_b = -\frac{5}{2}(J_0 - I_b) + \frac{12}{7}J_0' + \frac{7}{6}J_0'' - \frac{4}{7}J_0'''.$$

Since the governing fourth-order equation is exactly the same as the one for I_0 in Example 16.7, the solution is also the same,

$$J_0(\tau_y) = I_b + (I_{bw} - I_b)[C_1 \cosh \lambda_1 \tau_y + C_2 \cosh \lambda_2 \tau_y],$$

(here given right away without the C_3 and C_4, which are eliminated through the $\tau_y = 0$ boundary condition). Again,

$$C_1 = \frac{b_2 - a_2}{a_1 b_2 - a_2 b_1}, \qquad C_2 = \frac{a_1 - b_1}{a_1 b_2 - a_2 b_1},$$

but with the a_i and b_i replaced by

$$a_i = \left(\frac{5}{8} + \frac{1}{8}\lambda_i^2\right)\cosh \lambda_i \frac{\tau_L}{2} + \frac{2}{3}\lambda_i \sinh \lambda_i \frac{\tau_L}{2}, \qquad i = 1, 2,$$
$$b_i = \left(-\frac{5}{2} + \frac{7}{6}\lambda_i^2\right)\cosh \lambda_i \frac{\tau_L}{2} - \left(\frac{12}{7}\lambda_i - \frac{4}{7}\lambda_i^3\right)\sinh \lambda_i \frac{\tau_L}{2}, \qquad i = 1, 2.$$

The heat flux through the medium is determined from equation (16.89) as

$$q(\tau_y) = -\frac{4\pi}{3}\left(I_0' + \frac{2}{5}I_2'\right) = -\frac{4\pi}{3}J_0'.$$

Substituting for J_0 we may express the heat flux for a gray medium again in nondimensional form as

$$\Psi = \frac{q(\tau_y)}{n^2\sigma(T_w^4 - T^4)} = -\frac{4}{3}\sum_{i=1}^{2} C_i \lambda_i \sinh \lambda_i \tau_y.$$

As mentioned in the beginning of this section, for a one-dimensional slab the SP_N-method reduces to the regular P_N solution. Therefore, the solution here must be identical to that of Example 16.4, which can be shown to be true after considerable algebra.

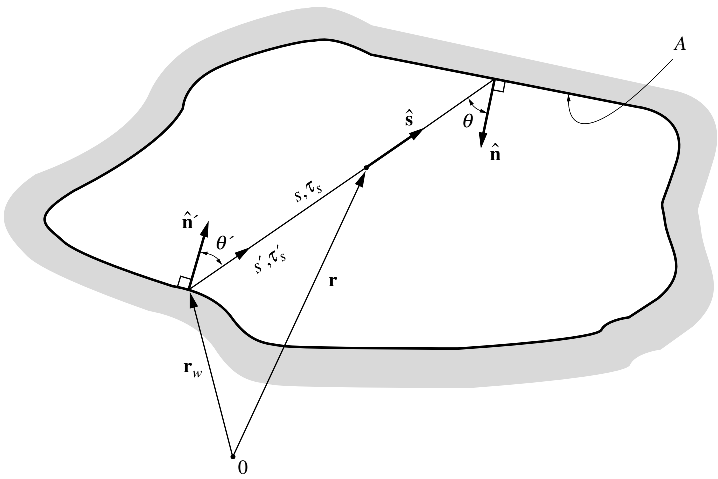

FIGURE 16-9
Radiative intensity within an arbitrary enclosure.

16.8 THE MODIFIED DIFFERENTIAL APPROXIMATION

As indicated earlier, the P_1- or *differential approximation* enjoys great popularity because of its relative simplicity and because of its compatibility with standard methods for the solution of the (overall) energy equation. The fact that the P_1-approximation may become very inaccurate in optically thin media—and thus of limited use—has prompted a number of investigators to seek enhancements or modifications to the differential approximation to make it reasonably accurate for all conditions [59–70]. We shall briefly describe here the so-called *modified differential approximation*.

The directional intensity at any given point inside the medium is due to two sources: radiation originating from a surface (due to emission and reflection), and radiation originating from within the medium (due to emission and in-scattering). The contribution due to radiation emanating from walls may display very irregular directional behavior, especially in optically thin situations (due to surface radiosities varying across the enclosure surface, causing irradiation to change rapidly over incoming directions). Intensity emanating from inside the medium generally varies very slowly with direction because emission and isotropic scattering result in an isotropic radiation source. Only for highly anisotropic scattering may the radiation source—and, therefore, at least locally also the intensity—display irregular directional behavior.

In what they termed the *modified differential approximation (MDA)* Olfe [59–62] and Glatt and Olfe [71] separated wall emission from medium emission in simple black and gray-walled enclosures with gray, nonscattering media, evaluating radiation due to wall emission with exact methods, and radiation from medium emission with the differential (or P_1) approximation. While very accurate, their model was limited to nonscattering media in simple, mostly one-dimensional enclosures. Wu and coworkers [63] demonstrated, for one-dimensional plane-parallel media, that the MDA may be extended to scattering media with reflecting boundaries. Finally, Modest [64] showed that the method can be applied to three-dimensional linear-anisotropically scattering media with reflecting boundaries. While until recently only used in conjunction with the P_1-approximation, higher order P_N- and SP_N-methods can also benefit from this approach, as recently shown by Modest and Yang [13], who demonstrated the accuracy of a modified P_3-approach.

Consider an arbitrary enclosure as shown in Fig. 16-9. The equation of transfer is, from equation (16.4),

$$\frac{dI}{d\tau_s}(\mathbf{r}, \hat{\mathbf{s}}) = \hat{\mathbf{s}} \cdot \nabla_\tau I = S(\mathbf{r}, \hat{\mathbf{s}}) - I(\mathbf{r}, \hat{\mathbf{s}}), \tag{16.101}$$

where, for linear-anisotropic scattering with a phase function given by equation (16.32), the radiative source term is, from equation (16.33),

$$S(\mathbf{r}, \hat{\mathbf{s}}) = (1-\omega) I_b(\mathbf{r}) + \frac{\omega}{4\pi}[G(\mathbf{r}) + A_1 \mathbf{q}(\mathbf{r}) \cdot \hat{\mathbf{s}}]. \tag{16.102}$$

For diffusely reflecting walls, equations (16.101) and (16.102) are subject to the boundary condition

$$I(\mathbf{r}_w, \hat{\mathbf{s}}) = \frac{J_w}{\pi}(\mathbf{r}_w) = I_{bw}(\mathbf{r}_w) - \frac{1-\epsilon}{\pi\epsilon}\mathbf{q} \cdot \hat{\mathbf{n}}(\mathbf{r}_w), \tag{16.103}$$

where J_w is the surface radiosity related to I_{bw} and $q_w = \mathbf{q} \cdot \hat{\mathbf{n}}$ through equation (16.46).

We now break up the intensity at any point into two components: one, I_w, which may be traced back to emission from the enclosure wall (but may have been attenuated by absorption and scattering in the medium, and by reflections from the enclosure walls), and the remainder, I_m, which may be traced back to the radiative source term (i.e., radiative intensity released within the medium into a given direction by emission and scattering). Thus, we write

$$I(\mathbf{r}, \hat{\mathbf{s}}) = I_w(\mathbf{r}, \hat{\mathbf{s}}) + I_m(\mathbf{r}, \hat{\mathbf{s}}) \tag{16.104}$$

and let I_w satisfy the equation

$$\frac{dI_w}{d\tau_s}(\mathbf{r}, \hat{\mathbf{s}}) = -I_w(\mathbf{r}, \hat{\mathbf{s}}), \tag{16.105}$$

leading to

$$I_w(\mathbf{r}, \hat{\mathbf{s}}) = \frac{J_w}{\pi}(\mathbf{r}_w)\, e^{-\tau_s}, \tag{16.106}$$

as indicated in Fig. 16-9. Since for I_w no radiative source within the medium is considered, the radiosity in equation (16.106) is the one caused by wall emission only (with attenuation within the medium). The radiosity variation along the enclosure wall may be determined by invoking the definition of the radiosity as the sum of emission plus reflected irradiation, or

$$\begin{aligned} J_w(\mathbf{r}) &= \epsilon\pi I_{bw}(\mathbf{r}) + (1-\epsilon)\int_{\hat{\mathbf{s}}\cdot\hat{\mathbf{n}}<0} I_w(\mathbf{r}, \hat{\mathbf{s}})\, |\hat{\mathbf{s}} \cdot \hat{\mathbf{n}}|\, d\Omega \\ &= \epsilon\pi I_{bw}(\mathbf{r}) + (1-\epsilon)\int_A J_w(\mathbf{r}_w)\frac{\cos\theta\cos\theta'}{\pi S^2}\, e^{-\tau_s}\, dA, \end{aligned} \tag{16.107}$$

as also indicated in Fig. 16-9. The surface integral representation of equation (16.107) is obtained by invoking the definition of solid angle, equation (1.29), or $d\Omega = \cos\theta'\, dA/S^2$, equivalent to the definition of view factors in Chapter 4.

Equation (16.107) is the standard integral equation for the radiosity in an enclosure without a participating medium, except for the attenuation factor $e^{-\tau_s}$, and may be solved by standard methods such as breaking up the enclosure surface into N small subsurfaces of constant radiosity. Assuming that the attenuation term may be approximated by the value between node centers leads to

$$J_i = \epsilon_i \pi I_{bi} + (1-\epsilon_i)\sum_{j=1}^{N} J_j\, e^{-\tau_{ij}} F_{i-j}, \qquad i = 1, 2, \ldots, N, \tag{16.108}$$

where the F_{i-j} are the view factors between the subsurfaces.

It remains to calculate the contribution to the intensity from within the medium. Assuming that the P_1-approximation adequately represents intensity emanating from within the medium, we write, using equation (16.31),

$$I_m(\mathbf{r}, \hat{\mathbf{s}}) \simeq \frac{1}{4\pi}[G_m(\mathbf{r}) + 3\mathbf{q}_m(\mathbf{r}) \cdot \hat{\mathbf{s}}], \tag{16.109}$$

where G_m and $\mathbf{q}_m$ are medium-related incident radiation and heat flux, respectively, defined by

$$G_m(\mathbf{r}) = \int_{4\pi} I_m(\mathbf{r}, \hat{\mathbf{s}})\, d\Omega, \tag{16.110}$$

$$\mathbf{q}_m(\mathbf{r}) = \int_{4\pi} I_m(\mathbf{r}, \hat{\mathbf{s}})\, \hat{\mathbf{s}}\, d\Omega. \tag{16.111}$$

Substituting equations (16.105) and (16.109) into equation (16.101) we get

$$\frac{dI_m}{d\tau_s} = \hat{\mathbf{s}} \cdot \nabla_\tau I_m \simeq (1-\omega)I_b + \frac{\omega}{4\pi}\left[G_w + G_m + A_1(\mathbf{q}_w + \mathbf{q}_m)\cdot\hat{\mathbf{s}}\right] - I_m, \tag{16.112}$$

where the wall-related incident radiation and heat flux are defined as

$$G_w(\mathbf{r}) = \int_{4\pi} I_w(\mathbf{r}, \hat{\mathbf{s}})\, d\Omega = \frac{1}{\pi}\int_{4\pi} J_w(\mathbf{r}_w)\, e^{-\tau_s}\, d\Omega, \tag{16.113}$$

$$\mathbf{q}_w(\mathbf{r}) = \int_{4\pi} I_w(\mathbf{r}, \hat{\mathbf{s}})\, \hat{\mathbf{s}}\, d\Omega = \frac{1}{\pi}\int_{4\pi} J_w(\mathbf{r}_w)\, e^{-\tau_s}\hat{\mathbf{s}}\, d\Omega. \tag{16.114}$$

After integrating equation (16.112) over all solid angles, we have

$$\nabla_\tau \cdot \mathbf{q}_m = (1-\omega)4\pi I_b + \omega(G_w + G_m) - G_m. \tag{16.115}$$

If equation (16.112) is multiplied by $\hat{\mathbf{s}}$ before integration over all directions, we get

$$\nabla_\tau G_m = A_1\omega(\mathbf{q}_w + \mathbf{q}_m) - 3\mathbf{q}_m. \tag{16.116}$$

Equations (16.115) and (16.116) are a complete set of equations for the unknowns G_m and $\mathbf{q}_m$. [For higher-order P_N-approximations, additional equations would need to be generated by multiplying equation (16.112) by successively higher-order harmonics before integration.] The necessary boundary conditions for equations (16.115) and (16.116) are found by making an energy balance for medium-related radiation at a point on the surface

$$q_m \cdot \hat{\mathbf{n}} = \epsilon \int_{\hat{\mathbf{s}}\cdot\hat{\mathbf{n}}<0} I_m(\mathbf{r}, \hat{\mathbf{s}})\, \hat{\mathbf{s}} \cdot \hat{\mathbf{n}}\, d\Omega, \tag{16.117}$$

which, after substituting equation (16.109) for I_m, leads to Marshak's boundary condition for a cold surface,

$$2\left(\frac{2}{\epsilon} - 1\right)\mathbf{q}_m \cdot \hat{\mathbf{n}} + G_m = 0. \tag{16.118}$$

[For a more detailed derivation of these relations see the similar development of the P_1-approximation, equations (16.34) through (16.37).] Equations (16.115) and (16.116), together with boundary condition (16.118), constitute a set of equations for the determination of the medium-related incident radiation and heat flux, with enclosure wall-related incident radiation and heat flux given by equations (16.113), (16.114), and (16.107). Finally, the total values for incident radiation and heat flux are given by

$$G = G_w + G_m, \tag{16.119}$$

$$\mathbf{q} = \mathbf{q}_w + \mathbf{q}_m. \tag{16.120}$$

This solution will reduce to the correct solution for the optically thin limit (where the medium-related contribution vanishes), and to the unmodified P_1-approximation for the optically thick limit. For nonscattering or isotropically scattering media, the method requires the solution to a Helmholtz equation (similar to the ordinary P_1-approximation), and the additional evaluation of

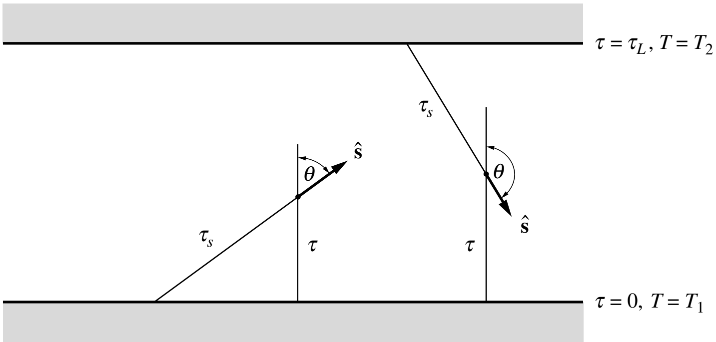

FIGURE 16-10
Intensities for a one-dimensional plane-parallel slab.

a scalar surface integral for every point in the medium (G_w); whereas, for anisotropic scattering, G_w as well as a vector surface integral ($\mathbf{q}_w$) must be evaluated. In addition, for the determination of radiosities, a surface integral equation must be solved (or view factors evaluated). If the extinction coefficient is independent of temperature, the G_w (and $\mathbf{q}_w$) integrals do not depend on medium temperature and, thus, may be evaluated once and for all (i.e., they will not enter any iterative process if the temperature field of the medium is to be determined). If the extinction coefficient is temperature dependent, a solution for G_w and $\mathbf{q}_w$, based on gross estimates for the temperature field [in order to calculate the optical distances τ_{ij} in equation (16.108)], still will result in the correct optically thin and thick limits and, therefore, can be expected to be of reasonable accuracy everywhere in between.

Example 16.9. Consider a one-dimensional, gray, absorbing/emitting and isotropically scattering slab with refractive index $n = 1$ at radiative equilibrium, contained between two isothermal black walls at temperatures T_1 and T_2, respectively. Determine the radiative heat flux between the plates using the modified differential approximation.

Solution
Measuring optical distance $\tau = \int_0^z \beta\, dz$ perpendicular to the plates, as shown in Fig. 16-10, one may readily determine the wall-related intensity as

$$I_w(\tau, \mu) = \begin{cases} \dfrac{\sigma T_1^4}{\pi} e^{-\tau/\mu}, & 0 < \mu \leq 1, \\ \dfrac{\sigma T_2^4}{\pi} e^{(\tau_L - \tau)/\mu}, & -1 \leq \mu < 0, \end{cases}$$

leading to

$$G_w(\tau) = 2\pi \int_{-1}^{1} I_w\, d\mu = 2\sigma T_1^4 E_2(\tau) + 2\sigma T_2^4 E_2(\tau_L - \tau),$$

$$q_w(\tau) = 2\pi \int_{-1}^{1} I_w\, d\mu = 2\sigma T_1^4 E_3(\tau) - 2\sigma T_2^4 E_3(\tau_L - \tau).$$

Substituting these expressions into equation (16.116) with $A_1 = 0$ and $q_m = q - q_w$ gives

$$\frac{dG_m}{d\tau} = -3q + 6\left[\sigma T_1^4 E_3(\tau) - \sigma T_2^4 E_3(\tau_L - \tau)\right].$$

Since $q =$ const, due to radiative equilibrium, this equation is readily integrated, and

$$G_m = C - 3q\tau - 6\left[\sigma T_1^4 E_4(\tau) + \sigma T_2^4 E_4(\tau_L - \tau)\right].$$

The constants C and q may be found from the boundary conditions, equation (16.118), or

$$\begin{aligned} \tau = 0: \quad 2q_m + G_m &= 2q - 2\sigma T_1^4 + 4\sigma T_2^4 E_3(\tau_L) + C - 2\sigma T_1^4 - 6\sigma T_2^4 E_4(\tau_L) = 0, \\ \tau = \tau_L: \quad -2q_m + G_m &= -2q + 4\sigma T_1^4 E_3(\tau_L) - 2\sigma T_2^4 + C - 3q\tau_L - 6\sigma T_1^4 E_4(\tau_L) - 2\sigma T_2^4 = 0. \end{aligned}$$

Subtracting the second boundary condition from the first yields the nondimensional heat flux as

$$\Psi = \frac{q}{\sigma(T_1^4 - T_2^4)} = \frac{1 + E_3(\tau_L) - \frac{3}{2}E_4(\tau_L)}{1 + 3\tau_L/4}.$$

Comparison with exact values from Table 14.1 as well as those from the *ordinary differential approximation (ODA)*, given in Example 15.5, shows that the ODA has a maximum error of $\approx 3.3\%$, compared with $\approx 1.3\%$ for the MDA (both near $\tau_L = 1$). This comparison, however, in no way demonstrates the power of the present method, since this problem is one of the very few in which the ordinary differential approximation actually reduces to the correct optically thin limit.

Example 16.10. Consider a one-dimensional, gray, absorbing/emitting, nonscattering slab between two isothermal black plates, both at temperature T_w. The medium has a refractive index of $n = 1$ and is isothermal at T_m. Determine the radiative heat flux between the plates using the MDA.

Solution
The wall-related heat flux follows immediately from the previous example as

$$q_w(\tau) = 2\sigma T_w^4[E_3(\tau) - E_3(\tau_L - \tau)].$$

For a nonscattering medium equations (16.115) and (16.116) contain no wall-related terms, and

$$\frac{d^2G_m}{d\tau^2} = -3\frac{dq_m}{d\tau} = -3(4\sigma T_m^4 - G_m),$$

or

$$G_m(\tau) = C_1\, e^{-\sqrt{3}\tau} + C_2\, e^{+\sqrt{3}\tau} + 4\sigma T_m^4 = C\left[e^{-\sqrt{3}\tau} + e^{-\sqrt{3}(\tau_L-\tau)}\right] + 4\sigma T_m^4,$$

where, in the last equation, we have used the fact that $G_m(\tau) = G_m(\tau_L - \tau)$, as a result of symmetry. The medium-related heat flux follows as

$$q_m = -\frac{1}{3}\frac{dG_m}{d\tau} = \frac{C}{\sqrt{3}}\left[e^{-\sqrt{3}\tau} - e^{-\sqrt{3}(\tau_L-\tau)}\right].$$

Applying the boundary condition at $\tau = 0$, we obtain

$$2q_m + G_m = \frac{2}{\sqrt{3}}C\left(1 - e^{-\sqrt{3}\tau_L}\right) + C\left(1 + e^{-\sqrt{3}\tau_L}\right) + 4\sigma T_m^4 = 0,$$

and

$$q_m(\tau) = -\frac{4\sigma T_m^4\left[e^{-\sqrt{3}\tau} - e^{-\sqrt{3}(\tau_L-\tau)}\right]}{2 + \sqrt{3} - (2 - \sqrt{3})\, e^{-\sqrt{3}\tau_L}}.$$

The total heat flux is evaluated as $q = q_w + q_m$. At the lower surface we have

$$q(0) = [1 - 2E_3(\tau_L)]\,\sigma T_w^4 - \frac{4\left(1 - e^{-\sqrt{3}\tau_L}\right)}{2 + \sqrt{3} - (2 - \sqrt{3})\, e^{-\sqrt{3}\tau_L}}\sigma T_m^4.$$

This example illustrates a remaining weakness of the MDA: While q goes to the correct optically thin limit ($q \to 0$), for the optically thick limit the term due to medium emission goes to the value predicted by the ODA, which is not equipped to handle temperature jumps within optically thick media. The result is not included in Fig. 16-8 since it may lie anywhere between the exact and the P_1 results, depending on the values of T_w and T_m.

Some multidimensional MDA examples have been given by [26, 28, 61, 64, 70–74], proving their excellent accuracy under all conditions (even when the P_1-approximation fails).

16.9 COMPARISON OF METHODS

To better understand the strengths and weaknesses of the various spherical harmonics methods we will present a few example results for three two-dimensional problems, i.e., a square enclosure with a purely scattering medium, a square enclosure with prescribed temperature and absorption coefficient fields, and a (realistic) axisymmetric flame.

Purely Scattering Medium We consider a square enclosure filled with a purely scattering medium, with gray and spatially constant scattering coefficient σ_s (or, equivalently, a gray

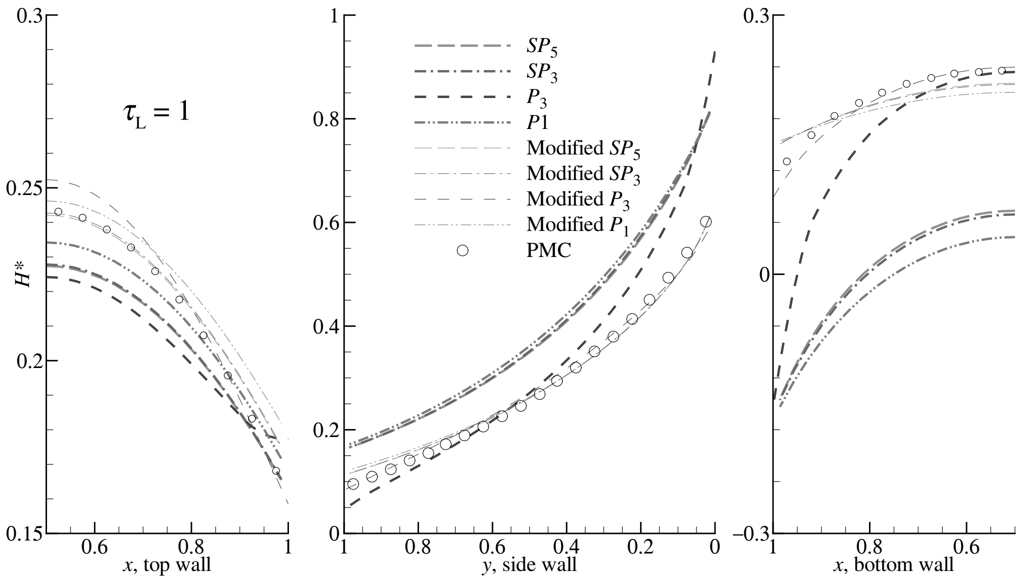

FIGURE 16-11
Comparison of various P_N and SP_N levels for surface heat fluxes in a purely scattering square enclosure; optically intermediate case $\tau_L = 1.0$.

medium at radiative equilibrium with constant extinction coefficient β). All four walls are black, and the bottom wall is at $T_w > 0$, while the other three walls are at 0 K. This type of problem has often been employed to show how so-called ray effects can adversely affect solutions obtained with the discrete ordinates method, which is the topic of the next chapter (see also Fig. 17-7). Figure 16-11 shows the normalized *incoming* irradiation $H^* = H/\sigma T_w^4$ (which must always be positive), for the top, side, and bottom walls for an optically intermediate case of $\tau_L = \sigma_s L = 1$, comparing results from P_1, P_3, SP_3, SP_5, and their modified versions to exact results obtained with the statistical Monte Carlo method (PMC, see Chapter 21). It is observed than none of the P_N and SP_N schemes gives very satisfactory results, even leading to physically impossible negative irradiation at the bottom wall. The modified versions (the scheme being applied to all *(S)P$_N$* levels) give very good results for all cases, for this surface-driven problem; the modifying scheme provides much greater improvements than going to a higher-order method. Careful observation shows that higher-order SP_N retain the character of the P_1 solution with only slight improvement. More detailed results are given in [13, 57], showing that the performance of the straight P_N and SP_N methods of all orders is very poor for optically thin situations, while modified P_1 (and higher orders) give essentially exact answers.

Medium with Variable Gray Properties. Next we will consider a square enclosure with the following nondimensional field [18, 57, 75]:

$$I_b = 1 + 5r^2(2 - r^2), \tag{16.121a}$$

$$\kappa = C_k\left[1 + \frac{15}{4}(2 - r^2)^2\right], \tag{16.121b}$$

with

$$r^2 = x^2 + y^2; \qquad -1 \le x \le +1, \quad -1 \le y \le +1, \tag{16.121c}$$

i.e., the blackbody intensity (Planck function) is normalized with its minimum value (obtained at the center and the four corners), with a maximum value of $I_b = 6$ at a distance of $r = 1$ from the centerline. The absorption coefficient, normalized in terms of length units, has a maximum value of $\kappa = 16C_k$ at $x = y = 0$, and rapidly diminishes away from the center to a minimum

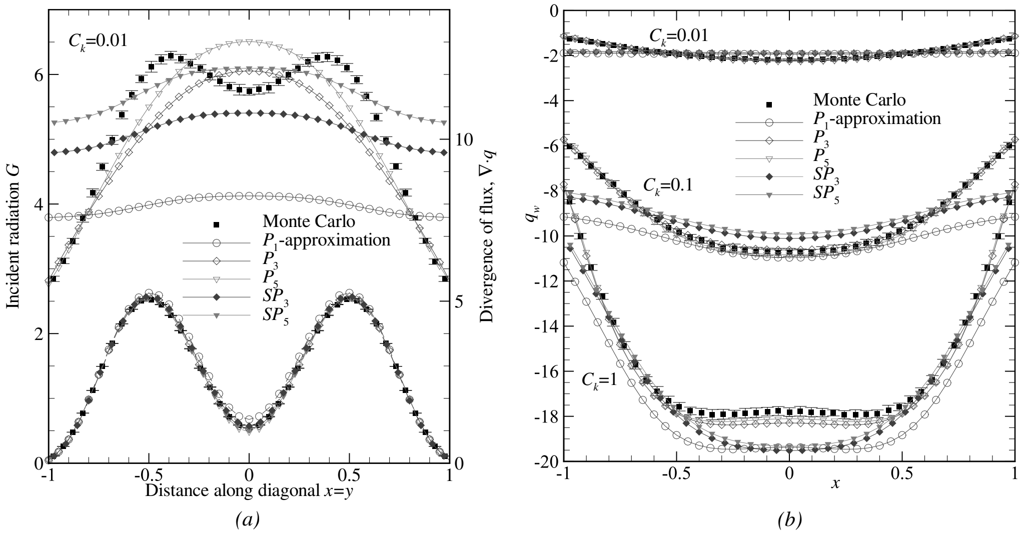

FIGURE 16-12
Square enclosure with variable properties: *(a)* incident radiation and radiative source for optically thin case (C_k = 0.01); *(b)* radiative flux along bottom wall ($y = -1$).

value of $\kappa = C_k$ at the four corners. Thus the problem is radially one-dimensional, except for the conditions at the four perpendicular walls, which are assumed cold and black. The optical thickness of the square enclosure is $\tau_D = 18\sqrt{2}C_k$ along a diagonal, and $\tau_L = 23.5C_k$ along an $x = 0$ or $y = 0$ line, respectively. Here we present the solutions for incident radiation and divergence of radiative flux for the case of $C_k = 0.01$ (optically thin conditions) in Fig. 16-12*a*. Again, we compare several levels of the P_N-approximation, with corresponding results from the SP_N-methods, and against exact Monte Carlo results. Since there is no wall emission, there are no modified P_N/SP_N results. It is observed that none of the methods can predict the double maximum for incident radiation, but P_3 considerably outperforms P_1, and P_5 gives better answers than P_3. While SP_3 and SP_5 are improvements over the P_1 results, their character remains similar to P_1. For intermediate and large optical thickness [57] all orders and methods rapidly become more accurate. All methods predict the divergence of the radiative flux well, with P_1 lagging a bit in accuracy; this remains true for larger optical thickness. Figure 16-12*b* shows radiative fluxes along the cold bottom wall for which, as expected, P_1 gives the worst results for the optically thick case ($C_k = 1$), because of the step in temperature at the wall. It is seen that P_3 and P_5 always give accurate results, while wall fluxes for P_1 may display inaccuracies in multidimensional geometries. SP_N solutions display P_1 character, i.e., lag in accuracy considerably behind their P_N counterpart.

Axisymmetric Nongray Flame As a final example we consider a realistic application in the form of an axisymmetric methane jet flame investigated in several studies [76, 77]. The flame is a scaled-up version of the much studied (but very small and, therefore, only weakly radiating) Sandia Flame D [78]. Figure 16-13*a* shows temperature and concentration contours for the flame, with extreme temperature and concentration gradients in the radial (and, to a lesser extent, the axial) direction, which are accompanied by similar gradients in absorption coefficient and blackbody intensity. In addition, the absorption coefficient of absorption gases is strongly nongray, i.e., the flame is optically thin-to-transparent across parts of the spectrum, and optically thick in other parts, and the concentration of water vapor peaks at an earlier axial location than temperature and carbon dioxide (because of formation of CO before reaction to CO_2 takes place). All this adds up to extreme challenges for the RTE solver (be it a spherical harmonics solver or one of the methods discussed in the following chapters) as well as the

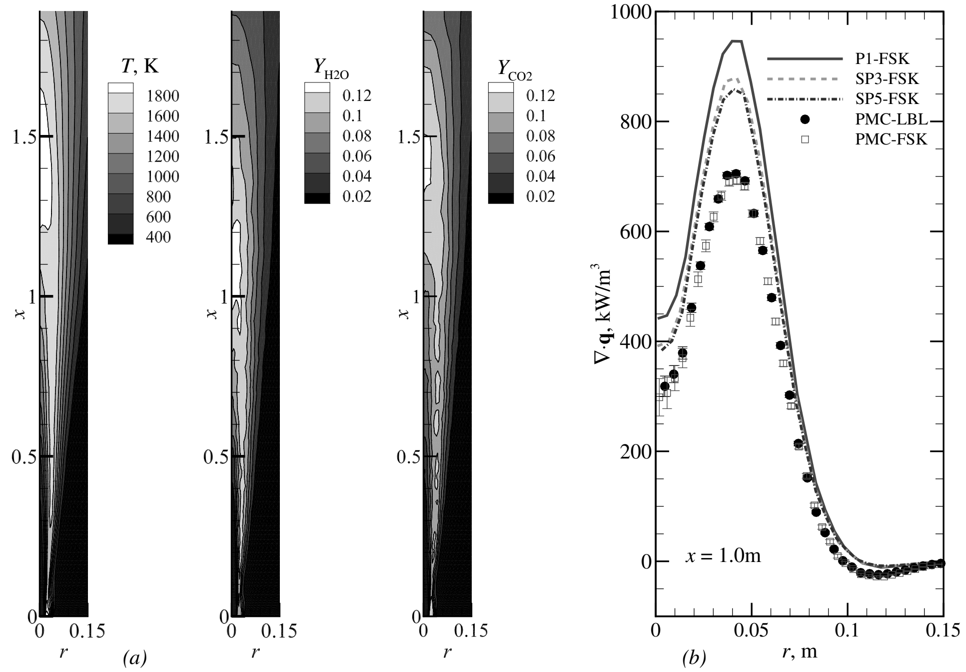

FIGURE 16-13
Two-dimensional axisymmetric methane jet flame with variable nongray properties: *(a)* contour maps of temperature and species mass fractions; *(b)* radiative source at fixed axial location (x = 1.0 m) as calculated by several methods.

spectral model. Figure 16-13*b* shows the negative radiative source, $\nabla \cdot \mathbf{q}$ for one axial location (with off-axis maximum temperature) as calculated by the P_1, SP_3, and SP_5 methods together with the the *Full Spectrum Correlated-k (FSCK)* spectral model (to be discussed in Section 20.10), and compared to exact Monte Carlo calculations. We note in passing that the FSCK spectral model incurs very little error, so that differences between the $(S)P_N$ solutions and Monte Carlo results are errors attributable to the $(S)P_N$ methods, which—for this extremely challenging case—peak at 35% (P_1), 25% (SP_3), and 20% (SP_5), respectively.

References

1. Jeans, J. H.: "The equations of radiative transfer of energy," *Monthly Notices Royal Astronomical Society*, vol. 78, pp. 28–36, 1917.
2. Kourganoff, V.: *Basic Methods in Transfer Problems*, Dover Publications, New York, 1963.
3. Davison, B.: *Neutron Transport Theory*, Oxford University Press, London, 1958.
4. Murray, R. L.: *Nuclear Reactor Physics*, Prentice Hall, Englewood Cliffs, NJ, 1957.
5. Gelbard, E. M.: "Simplified spherical harmonics equations and their use in shielding problems," Technical Report WAPD-T-1182, Bettis Atomic Power Laboratory, 1961.
6. Sommerfeld, A.: *Partial Differential Equations of Physics*, Academic Press, New York, 1964.
7. Krook, M.: "On the solution of the equation of transfer, I," *Astrophysical Journal*, vol. 122, pp. 488–497, 1955.
8. Cheng, P.: "Study of the flow of a radiating gas by a differential approximation," Ph.D. thesis, Stanford University, Stanford, CA, 1965.
9. Cheng, P.: "Dynamics of a radiating gas with application to flow over a wavy wall," *AIAA Journal*, vol. 4, no. 2, pp. 238–245, 1966.
10. Ou, S. C. S., and K. N. Liou: "Generalization of the spherical harmonic method to radiative transfer in multi-dimensional space," *Journal of Quantitative Spectroscopy and Radiative Transfer*, vol. 28, no. 4, pp. 271–288, 1982.
11. Condiff, D.: "Anisotropic scattering in three dimensional differential approximation of radiation heat transfer," in *Fundamentals and Applications of Radiation Heat Transfer*, vol. HTD-72, ASME, pp. 19–29, 1987.
12. Brenner, H.: "The Stokes resistance of a slightly deformed sphere — II intrinsic resistance operators for an arbitrary initial flow," *Chemical Engineering and Science*, vol. 22, p. 375, 1967.

13. Modest, M. F., and J. Yang: "Elliptic PDE formulation and boundary conditions of the spherical harmonics method of arbitrary order for general three-dimensional geometries," *Journal of Quantitative Spectroscopy and Radiative Transfer*, vol. 109, pp. 1641–1666, 2008.
14. Abramowitz, M., and I. A. Stegun (eds.): *Handbook of Mathematical Functions*, Dover Publications, New York, 1965.
15. Mark, J. C.: "The spherical harmonics method, Part I," Technical Report Atomic Energy Report No. MT 92, National Research Council of Canada, 1944.
16. Mark, J. C.: "The spherical harmonics method, Part II," Technical Report Atomic Energy Report No. MT 97, National Research Council of Canada, 1945.
17. Marshak, R. E.: "Note on the spherical harmonics method as applied to the Milne problem for a sphere," *Phys. Rev.*, vol. 71, pp. 443–446, 1947.
18. Modest, M. F.: "Further developments of the elliptic P_N-approximation formulation and its boundary conditions," *Numerical Heat Transfer – Part B: Fundamentals*, vol. 61, 2012, in print.
19. Pellaud, B.: "Numerical comparison of different types of vacuum boundary conditions for the P_N approximation," *Trans. Am. Nucl. Soc.*, vol. 9, pp. 434–435, 1966.
20. Schmidt, E., and E. M. Gelbard: "A double P_N method for spheres and cylinders," *Trans. Am. Nucl. Soc.*, vol. 9, pp. 432–433, 1966.
21. MacRobert, T. M.: *Spherical Harmonics*, 3rd ed., Pergamon Press, New York, 1967.
22. Modest, M. F.: "Photon-gas formulation of the differential approximation in radiative transfer," *Letters in Heat and Mass Transfer*, vol. 3, pp. 111–116, 1976.
23. Pipes, L. A., and L. R. Harvill: *Applied Mathematics for Engineers and Physicists*, McGraw-Hill, New York, 1970.
24. Bayazitoğlu, Y., and J. Higenyi: "The higher-order differential equations of radiative transfer: P_3 approximation," *AIAA Journal*, vol. 17, pp. 424–431, 1979.
25. Park, S. H., and S. S. Kim: "Thermophoretic deposition of absorbing, emitting and isotropically scattering particles in laminar tube flow with high particle mass loading," *International Journal of Heat and Mass Transfer*, vol. 36, no. 14, pp. 3477–3485, 1993.
26. Park, H. M., R. K. Ahluwalia, and K. H. Im: "Three-dimensional radiation in absorbing–emitting–scattering media using the modified differential approximation," *International Journal of Heat and Mass Transfer*, vol. 36, no. 5, pp. 1181–1189, 1993.
27. Kamiuto, K., and S. Saitoh: "Combined forced-convection and correlated–radiation heat transfer in cylindrical packed beds," *Journal of Thermophysics and Heat Transfer*, vol. 8, no. 1, pp. 119–124, 1994.
28. Ahluwalia, R. K., and K. H. Im: "Spectral radiative heat-transfer in coal furnaces using a hybrid technique," *Journal of the Institute of Energy*, vol. 67, pp. 23–29, 1994.
29. Kaminski, D. A., X. D. Fu, and M. K. Jensen: "Numerical and experimental analysis of combined convective and radiative heat transfer in laminar flow over a circular cylinder," *International Journal of Heat and Mass Transfer*, vol. 38, no. 17, pp. 3161–3169, 1995.
30. Tsukada, T., K. Kakinoki, M. Hozawa, and N. Imaishi: "Effect of internal radiation within crystal and melt on Czochralski crystal growth of oxide," *International Journal of Heat and Mass Transfer*, vol. 38, pp. 2707–2714, 1995.
31. Ezekoye, O. A., and Z. Zhang: "Convective and radiative coupling in a burner-supported diffusion flame," *Journal of Thermophysics and Heat Transfer*, vol. 11, no. 2, pp. 239–245, 1997.
32. Derby, J. J., S. Brandon, and A. G. Salinger: "The diffusion and P1 approximations for modeling buoyant flow of an optically thick fluid," *International Journal of Heat and Mass Transfer*, vol. 41, no. 11, pp. 1405–1415, 1998.
33. Bayazitoğlu, Y., and B. Y. Wang: "Wavelets in the solution of nongray radiative heat transfer equation," *ASME Journal of Heat Transfer*, vol. 120, no. 1, pp. 133–139, 1998.
34. Lin, T. H., and C. H. Chen: "Influence of two-dimensional gas phase radiation on downward flame spread," *Combustion Science and Technology*, vol. 141, no. 1, pp. 83–106, 1999.
35. Kuo, D. C., J. C. Morales, and K. S. Ball: "Combined natural convection and volumetric radiation in a horizontal annulus: spectral and finite volume predictions," *ASME Journal of Heat Transfer*, vol. 121, pp. 610–615, 1999.
36. Zheng, B., C. X. Lin, and M. A. Ebadian: "Combined laminar forced convection and thermal radiation in a helical pipe," *International Journal of Heat and Mass Transfer*, vol. 43, no. 7, pp. 1067–1078, 2000.
37. Li, G., and M. F. Modest: "A method to accelerate convergence and to preserve radiative energy balance in solving the P_1 equation by iterative methods," *ASME Journal of Heat Transfer*, vol. 124, no. 3, pp. 580–582, 2002.
38. Liu, F., J. Swithenbank, and E. S. Garbett: "The boundary condition of the P_N-approximation used to solve the radiative transfer equation," *International Journal of Heat and Mass Transfer*, vol. 35, pp. 2043–2052, 1992.
39. Su, B.: "More on boundary conditions for differential approximations," *Journal of Quantitative Spectroscopy and Radiative Transfer*, vol. 64, pp. 409–419, 2000.
40. Mengüç, M. P., and S. Subramaniam: "Radiative transfer through an inhomogeneous fly-ash cloud: Effects of temperature and wavelength dependent optical properties," *Numerical Heat Transfer – Part A: Applications*, vol. 21, no. 3, pp. 261–273, 1992.
41. Kofink, W.: "Complete spherical harmonics solution of the Boltzmann equation for neutron transport in homogeneous media with cylindrical geometry," *Nuclear Science and Engineering*, vol. 6, pp. 473–486, 1959.
42. Tong, T. W., and P. S. Swathi: "Radiative heat transfer in emitting–absorbing–scattering spherical media," *Journal of Thermophysics and Heat Transfer*, vol. 1, no. 2, pp. 162–170, 1987.
43. Li, W., and T. W. Tong: "Radiative heat transfer in isothermal spherical media," *Journal of Quantitative Spectroscopy and Radiative Transfer*, vol. 43, no. 3, pp. 239–251, 1990.

44. Tong, T. W., and W. Li: "Enhancement of thermal emission from porous radiant burners," *Journal of Quantitative Spectroscopy and Radiative Transfer*, vol. 53, no. 2, pp. 235–248, 1995.
45. Wu, J. W., and H. S. Chu: "Combined conduction and radiation heat transfer in plane-parallel packed beds with variable porosity," *Journal of Quantitative Spectroscopy and Radiative Transfer*, vol. 61, no. 4, pp. 443–452, 1999.
46. Mengüç, M. P., and R. Viskanta: "Radiative transfer in three-dimensional rectangular enclosures containing inhomogeneous, anisotropically scattering media," *Journal of Quantitative Spectroscopy and Radiative Transfer*, vol. 33, no. 6, pp. 533–549, 1985.
47. Mengüç, M. P., and R. Viskanta: "Radiative transfer in axisymmetric, finite cylindrical enclosures," *ASME Journal of Heat Transfer*, vol. 108, pp. 271–276, 1986.
48. Yang, J., and M. F. Modest: "High-order *P-N* approximation for radiative transfer in arbitrary geometries," *Journal of Quantitative Spectroscopy and Radiative Transfer*, vol. 104, no. 2, pp. 217–227, 2007.
49. Varshalovich, D. A., A. N. Moskalev, and V. K. Khersonskii: *Quantum Theory of Angular Momentum*, World Scientific, Singapore, 1981.
50. Blanco, M. A., M. Flórez, and M. Bermejo: "Evaluation of the rotation matrices in the basis of real spherical harmonics," *Journal of Molecular Structure (Theochem)*, vol. 49, pp. 19–27, 1997.
51. *FlexPDE software*, PDE Solutions Inc., Antioch.
52. Sewell, G.: *PDE2D 9.0* http://www.pde2d.com/.
53. Schönauer, W.: *FDEM* see the "Fuel Cell Report" at http://www.rz.uni-karlsruhe.de/produkte/5336.php, 2005.
54. Larsen, E., J. E. Morel, and J. McGhee: "Simplified P_N approximations to the equations of radiative heat transfer and applications," in *Proceedings of the Joint International Conference on Mathematical Methods and Supercomputing in Nuclear Applications*, Portland, Oregon, 1993.
55. Pomraning, G. C.: "Asymptotic and variational derivations of the simplified p_n equations," *Annals of Nuclear Energy*, vol. 20, no. 9, pp. 623–637, 1993.
56. McClarren, R. G.: "Theoretical aspects of the simplified P_n equations," *Transport Theory and Statistical Physics*, vol. 39, pp. 73–109, 2011.
57. Modest, M. F., and S. Lei: "Simplified spherical harmonics method for radiative heat transfer," in *Proceedings of Eurotherm Seminar 95*, Elsevier, Nancy, France, April 2012.
58. Larsen, E., G. Thömmes, A. Klar, M. Seaïd, and T. Götz: "Asymptotic derivation of the simplified P_N equations," *Journal of Computational Physics*, vol. 183, pp. 652–675, 2002.
59. Olfe, D. B.: "A modification of the differential approximation for radiative transfer," *AIAA Journal*, vol. 5, no. 4, pp. 638–643, 1967.
60. Olfe, D. B.: "Application of a modified differential approximation to radiative transfer in a gray medium between concentric sphere and cylinders," *Journal of Quantitative Spectroscopy and Radiative Transfer*, vol. 8, pp. 899–907, 1968.
61. Olfe, D. B.: "Radiative equilibrium of a gray medium bounded by nonisothermal walls," *Progress in Astronautics and Aeronautics*, vol. 23, pp. 295–317, 1970.
62. Olfe, D. B.: "Radiative equilibrium of a gray medium in a rectangular enclosure," *Journal of Quantitative Spectroscopy and Radiative Transfer*, vol. 13, pp. 881–895, 1973.
63. Wu, C. Y., W. H. Sutton, and T. J. Love: "Successive improvement of the modified differential approximation in radiative heat transfer," *Journal of Thermophysics and Heat Transfer*, vol. 1, no. 4, pp. 296–300, 1987.
64. Modest, M. F.: "The modified differential approximation for radiative transfer in general three-dimensional media," *Journal of Thermophysics and Heat Transfer*, vol. 3, no. 3, pp. 283–288, 1989.
65. Modest, M. F.: "Two-dimensional radiative equilibrium of a gray medium in a plane layer bounded by gray non-isothermal walls," *ASME Journal of Heat Transfer*, vol. 96C, pp. 483–488, 1974.
66. Modest, M. F.: "Radiative equilibrium in a rectangular enclosure bounded by gray non-isothermal walls," *Journal of Quantitative Spectroscopy and Radiative Transfer*, vol. 15, pp. 445–461, 1975.
67. Modest, M. F., and D. Stevens: "Two dimensional radiative equilibrium of a gray medium between concentric cylinders," *Journal of Quantitative Spectroscopy and Radiative Transfer*, vol. 19, pp. 353–365, 1978.
68. Modest, M. F.: "The improved differential approximation for radiative transfer in general three-dimensional media," in *Heat Transfer Phenomena in Radiation, Combustion and Fires*, vol. HTD-106, ASME, pp. 213–220, 1989.
69. Modest, M. F.: "The improved differential approximation for radiative transfer in multi-dimensional media," *ASME Journal of Heat Transfer*, vol. 112, pp. 819–821, 1990.
70. Modest, M. F., and G. Pal: "Advanced differential approximation formulation of the p_n method for radiative transfer," in *Proceedings of ASME Summer Heat Transfer Conference, Paper HT2009-88242*, 2009.
71. Glatt, L., and D. B. Olfe: "Radiative equilibrium of a gray medium in a rectangular enclosure," *Journal of Quantitative Spectroscopy and Radiative Transfer*, vol. 13, pp. 881–895, 1973.
72. Hartung, L., and H. A. Hassan: "Radiation transport around axisymmetric blunt body vehicles using a modified differential approximation," *Journal of Thermophysics and Heat Transfer*, vol. 7, no. 2, pp. 220–227, 1993.
73. Wu, C. Y., and N. R. Ou: "Transient two-dimensional radiative and conductive heat transfer in a scattering medium," *International Journal of Heat and Mass Transfer*, vol. 37, no. 17, pp. 2675–2686, 1994.
74. Ravishankar, M., S. Mazumder, and M. Sankar: "Application of the modified differential approximation for radiative transfer to arbitrary geometry," *Journal of Quantitative Spectroscopy and Radiative Transfer*, vol. 111, no. 14, pp. 2052–2069, 2008.
75. Deshmukh, K. V., M. F. Modest, and D. C. Haworth: "Higher-order spherical harmonics to model radiation in direct numerical simulation of turbulent reacting flows," *Computational Thermal Sciences*, vol. 1, pp. 207–230, 2009.

76. Wang, A., M. F. Modest, D. C. Haworth, and L. Wang: "Monte Carlo simulation of radiative heat transfer and turbulence interactions in methane/air jet flames," *Journal of Quantitative Spectroscopy and Radiative Transfer*, vol. 109, no. 2, pp. 269–279, 2008.
77. Pal, G., A. Gupta, M. F. Modest, and D. C. Haworth: "Comparison of accuracy and computational expense of radiation models in simulation of non-premixed turbulent jet flames," in *Proceedings of 2011 ASME/JSME Thermal Engineering Joint Conference*, 2011.
78. Barlow, R. S.: *International Workshop on Measurement and Computation of Turbulent Nonpremixed Flames (TNF)* website: http://www.sandia.gov/TNF/abstract.html.

Problems

16.1 Consider a gray medium at radiative equilibrium contained within a long black cylinder with a surface temperature of $T(r = R, z) = T_w(z)$. Find the relevant boundary conditions for the P_1-approximation directly from equation (16.23), i.e., in a manner similar to the development in Example 16.1.

16.2 Consider a gray, isotropically scattering medium at radiative equilibrium contained between large, isothermal, gray plates at temperatures T_1 and T_2, and emittances ϵ_1 and ϵ_2, respectively. Determine the radiative heat flux between the plates using the P_1-approximation. Compare the result with the exact answer from Table 14.1.

16.3 Consider a large, isothermal (temperature T_w), gray and diffuse (emittance ϵ) wall adjacent to a semi-infinite gray absorbing/emitting and linear-anisotropically scattering medium. The medium is isothermal (temperature T_m). Determine the radiative heat flux as a function of distance away from the plate using the P_1-approximation with (*i*) Marshak's, (*ii*) Mark's boundary conditions.

16.4 Consider parallel, gray-diffuse plates, that are isothermal at temperatures T_1 and T_2, and with emittances ϵ_1 and ϵ_2, respectively. The plates are separated by a gray, linear-anisotropically scattering medium of thickness L, which is at radiative equilibrium. Using the P_1-approximation, determine the temperature distribution within, and the heat flux through, the medium. Compare the heat flux with the exact answer given by Table 14.1 (for isotropic scattering, and optical thicknesses of $\tau_L = \beta L = 0,\ 0.1,\ 0.5, 1, 2$, and 5). Show that the radiative heat flux can be obtained from the expression given in Example 16.3, by letting $R_2 = R_1 + L \to \infty$.

16.5 Black spherical particles of 100 μm radius are suspended between two cold and black parallel plates 1 m apart. The particles produce heat at a rate of $\pi/10$ W/particle, which must be removed by thermal radiation. The number of particles between the plates is given by

$$N_T(z) = N_0 + \Delta N z/L, \quad 0 < z < L; \qquad N_0 = \Delta N = 212 \text{ particles/cm}^3.$$

(*a*) Determine the local absorption coefficient and the local heat production rate; introduce an optical coordinate and determine the optical thickness of the entire gap.

(*b*) Assuming the P_1-approximation to be valid, what are the relevant equations and boundary conditions governing the heat transfer?

(*c*) What are the heat flux rates at the top and bottom surfaces? What is the entire amount of energy released by the particles? What is the maximum particle temperature?

16.6 Consider parallel, black plates spaced 1 m apart, at constant temperatures $T_1 = 1000$ K and $T_2 = 300$ K, respectively, separated by a gray, nonscattering medium at radiative equilibrium. The absorption coefficient of the medium depends on its temperature according to a power law, $\kappa = \kappa_0(T/T_0)^n$ ($\kappa_0 = 1\,\text{m}^{-1}$, $T_0 = 300$ K, and n is an arbitrary, positive constant).

(*a*) Using the P_1-approximation, outline how to determine the radiative heat flux through, and temperature field within, the medium (i.e., the result may contain unsolved implicit relationships).

(*b*) Write a small computer program to quantify the results for $n = 0,\ 0.5,\ 1$, and 4. Compare with results obtained for a constant κ [evaluated at an average temperature $T_{\text{av}} = 0.5 \times (300{+}1000) = 650$ K].

16.7 A gas/soot/coal mixture, which may be approximated as a gray, nonscattering medium with $\kappa = 1.317\,\mathrm{m}^{-1}$, is burning inside a spherical container of diameter $D = 1$ m, which has black and cold walls. During combustion the coal particles release heat uniformly at a rate of $\dot{Q}''' = 2.885\,\mathrm{MW/m^3}$ (per total volume of container). The mixture remains at radiative equilibrium throughout the combustion process. Set up the necessary equations and boundary conditions to find the medium's temperature distribution and total heat loss rate, assuming the P_1-approximation to hold.

16.8 Given the soot distribution of Problem 12.16, it is found that soot is generated where combustion takes place, i.e., the local heat release due to combustion may be written as $\dot{Q}'''(z) = \dot{Q}_0'''[1 - (z/L)^2]$, $\dot{Q}_0''' = 10^5\,\mathrm{W/m^3}$. Assuming the soot to be nonscattering and gray (with properties evaluated at $\lambda = 3\,\mu$m) and conduction/convection to be negligible, and the walls to be cold and black, determine the temperature distribution within the medium using the P_1/differential approximation.

16.9 Two infinitely long concentric cylinders of radii R_1 and R_2 with emittances ϵ_1 and ϵ_2 both have the same constant surface temperature T_w. The medium between the cylinders has a constant absorption coefficient κ and does not scatter; uniform heat generation $\dot{Q}'''$ takes place inside the medium. Determine the temperature distribution in the medium and heat fluxes at the wall if radiation is the only means of heat transfer by using the P_1-approximation.

16.10 An infinite, black, isothermal plate bounds a semi-infinite space filled with black spheres. At any given distance, z, away from the plate the particle number density is identical, namely $N_T = 6.3662\times10^8\,\mathrm{m}^{-3}$. However, the radius of the suspended spheres diminishes monotonically away from the surface as

$$a = a_o\, e^{-z/L}; \qquad a_o = 10^{-4}\,\mathrm{m}, \qquad L = 1\,\mathrm{m}.$$

(*a*) Determine the absorption coefficient as a function of z (you may make the large-particle assumption).

(*b*) Determine the optical coordinate as a function of z. What is the total optical thickness of the semi-infinite space?

(*c*) Assuming that radiative equilibrium prevails and that the differential approximation is valid, set up the boundary conditions.

(*d*) Solve for heat flux and temperature distribution (as a function of z).

16.11 Consider two parallel black plates both at 1000 K, which are 2 m apart. The medium between the plates emits and absorbs (but does not scatter) with an absorption coefficient of $\kappa = 0.05236\,\mathrm{cm}^{-1}$ (gray medium). Heat is generated by the medium according to the formula

$$\dot{Q}''' = C\sigma T^4, \qquad C = 6.958\times10^{-4}\,\mathrm{cm}^{-1},$$

where T is the local temperature of the medium between the plates. Assuming that radiation is the only important mode of heat transfer, determine the heat flux to the plates.

16.12 A furnace burning pulverized coal may be approximated by a gray cylinder at radiative equilibrium with uniform heat generation $\dot{Q}''' = 0.266\,\mathrm{W/cm^3}$, bounded by a cold black wall. The gray and constant absorption and scattering coefficients are, respectively, $0.16\,\mathrm{cm}^{-1}$ and $0.04\,\mathrm{cm}^{-1}$, while the furnace radius is $R = 0.5$ m. Scattering may be assumed to be isotropic. Using the P_1-approximation:

(*a*) Set up the relevant equations and their boundary conditions.

(*b*) Calculate the total heat loss from the furnace (per unit length).

(*c*) Calculate the radial temperature distribution; what are the centerline and adjacent-to-wall temperatures, respectively?

(*d*) Qualitatively, keeping the extinction coefficient constant, what is the effect of varying the scattering coefficient on (*i*) heat transfer rates, (*ii*) temperature levels?

16.13 The coal particles of Problem 12.3 are burnt in a long cylindrical combustion chamber of $R = 1$ m radius. The combustor walls are gray and diffuse, with $\epsilon_w = 0.8$, and are at 800 K. Since it is well stirred, combustion results in uniform heat generation throughout of $\dot{Q}''' = 720\,\mathrm{kW/m^3}$. Determine the maximum temperature in the combustor, using the P_1/differential approximation, assuming radiation is the only mode of heat transfer (use $\kappa = 4.5\,\mathrm{m}^{-1}$ and $\sigma_s = 0.5\,\mathrm{m}^{-1}$ if the results of Problem 12.3 are not available).

16.14 Estimate the radial temperature distribution in the sun. You may make the following assumptions:

(*i*) The sun is a sphere of radius R.
(*ii*) As a result of high temperatures in the sun the absorption and scattering coefficients may be approximated to be constant, i.e., κ_ν, β_ν = const $\neq f(\nu, T, r)$ (free–free transitions!).
(*iii*) Due to high temperatures, radiation is the only mode of heat transfer.
(*iv*) The fusion process may be approximated by assuming that a small sphere at the center of the sun releases heat uniformly corresponding to the total heat loss of the sun (i.e., assume the sun to be concentric spheres with a certain heat flux at the inner boundary $r = r_i$).

(*a*) Relate the heat production to the effective sun temperature $T_{\text{SHMeff}} = 5777\,\text{K}$.
(*b*) Would you expect the sun to be optically thin, intermediate, or thick? Why? What are the prevailing boundary conditions?
(*c*) Find an expression for the temperature distribution (for $r > r_i$).
(*d*) What is the surface temperature of the sun?

16.15 Repeat Problem 16.14 but replace assumption (*iv*) by the following: The fusion process may be approximated by assuming that the sun releases heat uniformly throughout its volume corresponding to the total heat loss of the sun.

16.16 Consider a sphere of very hot dissociated gas of radius 5 cm. The gas may be approximated as a gray, linear-anisotropically scattering medium with $\kappa = 0.1\,\text{cm}^{-1}$, $\sigma_s = 0.2\,\text{cm}^{-1}$, $A_1 = 1$. The gas is suspended magnetically in vacuum within a large cold container and is initially at a uniform temperature $T_g = 10{,}000\,\text{K}$. Using the P_1-approximation and neglecting conduction and convection, specify the total heat loss per unit time from the entire sphere at time $t = 0$. Outline the solution procedure for times $t > 0$.
Hint: Solve the governing equation by introducing a new dependent variable $g(\tau) = \tau(4\pi I_b - G)$.

16.17 A spherical test bomb of 1 m radius is coated with a nonreflective material and cooled. Inside the sphere is nitrogen mixed with spherical particles at a rate of 10^8 particles/m^3. The particles have a radius of 300 μm, are diffuse-gray with $\epsilon = 0.5$, and generate heat at a rate of 150 W/cm^3 of particle volume. Using absorption and scattering coefficients found in Problem 12.12, determine the temperature distribution inside the bomb, using the P_1-approximation and two simplified phase functions:

(*i*) isotropic scattering, and
(*ii*) linear-anisotropic back scattering with $A_1 = -1$.

In particular, what is the gas temperature at the center and at the wall? How much do the two scattering treatments differ from one another?

16.18 A revolutionary new fuel is ground up into small particles, magnetically confined to remain within a spherical cloud of radius R. This cloud of particles has a constant, gray absorption coefficient, does not scatter, and releases heat uniformly at $\dot{Q}'''$ (W/m^3). The cloud is suspended in a vacuum chamber, enclosed by a large, isothermal chamber (at T_w). Heat transfer is solely by radiation, i.e., $\nabla\cdot\mathbf{q} = \left(1/r^2\right) d\left(r^2 q\right)/dr = \dot{Q}'''$.

(*a*) Assuming the P_1-approximation to be valid, set up the necessary equations and boundary conditions to determine the heat transfer rates, and temperature distribution within the spherical cloud.
(*b*) Determine the maximum temperature in the cloud.

16.19 Repeat Problem 16.5 using subroutine `P1sor` and/or program `P1-2D`. How do the answers change for a quadratic enclosure (side walls also cold and black)?

16.20 Repeat Problem 16.6 using subroutine `P1sor` and/or program `P1-2D`. How do the answers change for a quadratic enclosure (side walls also black, with a linear surface temperature variation from $T(x = 0) = T_1$ to $T(x = L) = T_2$)?

16.21 Consider a gray, isotropically scattering medium at radiative equilibrium contained between large, isothermal, gray plates at temperatures T_1 and T_2, and emittances ϵ_1 and ϵ_2, respectively. Determine the radiative heat flux between the plates using the P_3-approximation. Compare the results with the answer from Problem 16.2.

16.22 Do Problem 16.3 using the P_3-approximation with Marshak's boundary condition.

16.23 A hot gray medium is contained between two concentric black spheres of radius $R_1 = 10\,\mathrm{cm}$ and $R_2 = 20\,\mathrm{cm}$. The surfaces of the spheres are isothermal at $T_1 = 2000\,\mathrm{K}$ and $T_2 = 500\,\mathrm{K}$, respectively. The medium absorbs and emits with $n = 1$, $\kappa = 0.05\,\mathrm{cm}^{-1}$, but does not scatter radiation. Determine the heat flux between the spheres using the modified differential approximation (MDA).
Note: This problem requires the numerical solution of a simple ordinary differential equation.

16.24 Repeat Problem 16.23 for concentric cylinders of the same radii. Compare your result with those of Fig. 16-5.
Note: This problem requires the numerical solution of a simple ordinary differential equation.